Title
SELF-FOCUSING AND SMALL-SCALE FILAMENT OF LIGHT IN LIQUIDS

Author
Loy, Michael M.T.

Publication Date
1971-05-01

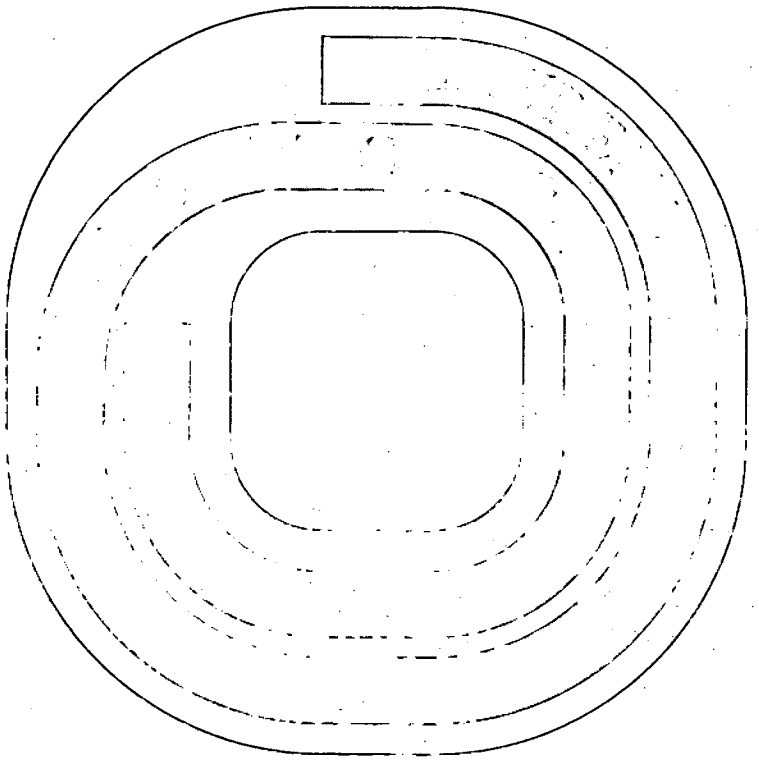

SELF-FOCUSING AND SMALL-SCALE FILAMENT OF LIGHT IN LIQUIDS

Michael M. T. Loy

(Ph. D. Thesis)

May 1971

AEC Contract No. W-7405-eng-48

DISCLAIMER

SELF-FOCUSING AND SMALL-SCALE FILAMENT OF LIGHT IN LIQUIDS

Contents

SELF-FOCUSING AND SMALL-SCALE FILAMENT OF LIGHT IN LIQUIDS

Michael M. T. Loy*

Department of Physics, University of California
and
Inorganic Materials Research Division, Lawrence Radiation Laboratory,
Berkeley, California

ABSTRACT

Experiments showed that the small-scale filaments obtained with a single-mode, Q-switched laser were actually tracks of moving focal spots. We observed that, under appropriate conditions, the focal spot might move forward and have a velocity faster than the light velocity in agreement with theoretical predictions. As a result of its high intensity, the moving focal spot leaves behind it a track of field-induced refractive index Δn which lasts over a period of the order of the relaxation time. Light trailing after the forward-moving focal spot can therefore be partially trapped by this moving optical waveguide. Due to the time variation of Δn and the trapping length, light emitted from the filament is phase-modulated and shows a large spectral broadening. The model is successful in explaining many observations on filaments.

---

*IBM Fellow

I. INTRODUCTION

Among the many non-linear optical effects studied recently, the problem of self-focusing and small-scale filaments of light occupies a special position. It is a fascinating physical phenomena in its own right. In addition, many interesting non-linear processes, such as stimulated Raman scattering, stimulated Brillouin scattering, and self-phase modulation, etc., are known to be induced by the high field intensity in the filament. A complete understanding of these phenomena is not possible without a valid model for the small-scale filaments that initiate them.

Askarjan,[1] Talanov,[2] and Chiao, Garmire, and Townes,[3] were the first ones to point out the possibility of an intense electromagnetic wave forming its own dielectric waveguide in a nonlinear medium with an intensity dependent refractive index, $n = n_o + n_2|E|^2$. They showed that for a beam with finite cross section, the diffraction effect can be compensated for by the induced nonlinear refractive index provided the beam power is equal to a threshold value given by $P_T = 5.763 \frac{\lambda^2 C'}{16\pi^3 n_2}$ where λ is the wavelength of light, C' is velocity of light. For CS_2, $P_{cr} \simeq 10$ kW. This effect is known as self-trapping. Subsequently, Kelley,[4] Talanov,[5] and Akhmanov, Sukhorukov, and Khokhlov[6] showed that for input power higher than P_{cr}, the focusing effect from the induced refractive index change overcomes the diffraction effect, and self-focusing occurs.

Experiments[7-9] were found to largely confirm the above theoretical analysis for self-focusing. It was also observed by Chiao,[10] et al. and Brewer[11] et al. that after self-focusing has occurred, small dots of a few microns in diameter appeared at the exit window of the liquid cell, persisting for a large range of cell lengths. The size of these

dots appeared to be a property of the liquid medium, about 5μ in CS_2. From the side of the cell, streaks of a few microns in diameter were also observed.[11] These streaks are called small-scale light filaments by Chiao et al.[10] The duration and energy of each filament were measured[12] to be about 1 nsec. and about 10 ergs respectively.

It was suggested[10-12] that self-trapping as described earlier is responsible for the observed small-scale filaments. Theoretical attempts to explain the diameter of the self-trapped filament, however, were not successful,[13-15] and it was not clear how the self-focusing beam can turn into a filament (or filaments).[14,15] It was suggested[16] that filament formation might be due to intensity fluctuations of the laser beam.

A different model for small-scale filament was, however, proposed by Lugovoi and Prokhorov,[17] who suggested that the small-scale filaments might simply be tracks of moving focal spots, in accordance with time variation of the input laser intensity. This moving focus model also predicted qualitatively all the filament properties mentioned earlier (see Section II for more details).

Experimentally, results from studying frequency broadening of light from filaments produced by multi-mode Q-switched lasers[18] or mode-locked[19] lasers seemed to support the self-trapping model. On the other hand, experiments using single-mode Q-switched lasers[20] definitely show that filaments are moving focal spots. It was apparent that filaments under different input conditions have different properties in certain respects. If a model is correct, it should be able to take into account the various input conditions in different experiments.

Recently, we proposed that while self-focusing of an input laser pulse should indeed yield a moving focal spot, light diffracting

after the focal spot can be partially trapped over an appreciable length in the dielectric waveguide established, not by its own power, but by the forward moving focal spot with velocity slightly faster than light velocity.[21] Calculations based on this picture give predictions in agreement with essentially all observed properties of filaments reported in the literature, including the spectral broadening of light from filaments at various input conditions.

In this work, we report the results of our systematic study of small-scale filaments. In Section II, the various theoretical descriptions of filaments are given, and we examine how well they can explain the properties of filaments. We also show how we can obtain spectral broadening using the moving focal spot model. In Section III, we describe our experiments using lasers with controlled input conditions, and show that the experimental results can only be explained using the moving focal spot model. Discussions and conclusions are presented in Section IV.

II. THEORETICAL DESCRIPTION OF SMALL-SCALE FILAMENTS

In this section, we review the theoretical calculations on self-focusing and see the approximations made in them. Then, for the small-scale filaments, we introduce the model of self-trapped filament, and the model of moving focal spots. We shall discuss how these models account for the known properties of filaments.

A. Review of Self-Trapping and Self-Focusing in Nonlinear Medium

1. Non-linear Medium

We consider an isotropic medium whose refractive index (or dielectric constant) is intensity-dependent and can be written as

$$n(E) = n_o + \Delta n$$

where n_o is the linear refractive index, E is the electric field, and

Δn is the induced refractive index change. In the steady state, we have

$$\Delta n = \Delta n_o = n_2|E|^2 + n_4|E|^4 + \ldots \qquad (1)$$

where the odd power terms vanish due to inversion symmetry.

The physical mechanisms behind the field-induced refractive index[3,19] could be molecular re-orientation, electrostriction, deformation of electron clouds around nuclei and "rocking" of molecules. In experiments to be discussed in this work where the input pulse duration is in the range of nanoseconds, molecular reorientation effect often dominates. The magnitude of n_2 ranges from 10^{-11} to 10^{-13} esu. In all of the media to be considered in this work, Δn is positive.

If we consider the dominant molecular reorientation mechanism only, the non-linear medium can be approximated by an ensemble of independent alignable symmetric top molecules (such as CS_2), whose polarizability along the symmetry axis α_1 is larger than that normal to the axis, α_1.[12-14] In the presence of an electric field the molecules tend to align their axes along the direction of the field, and thus increase the average polarizability of the medium, $\langle \alpha \rangle$. Using this model to calculate $\langle \alpha \rangle$ in the presence of an electric field E, and the Lorenz-Lorentz relation $(n^2-1)/(n^2+2) = \frac{4}{3}\pi N \langle \alpha \rangle$ where N is the number of molecules per unit volume, the steady-state Δn_o can be obtained,

$$\Delta n_o = \frac{(n_o^2+2)^2}{6n_o}\left(\frac{4}{3}\pi N\right)(\alpha_\parallel - \alpha_1) \times \left(\frac{4a}{45} + \frac{8a^2}{945} - \frac{16a^3}{14175} + \ldots\right) \qquad (2)$$

where $a = (\alpha_\parallel - \alpha_1)\langle E^2 \rangle / 2\,kT$; $\langle E^2 \rangle$ the time averaged intensity. From

this expression we can obtain the steady state non-linear coefficient n_2, n_4, n_6 ... in Eq. (1). According to this model, saturation of the refractive index change occurs when all the molecules are completely aligned with the field. For CS_2, this corresponds to $\Delta n_o = 0.5$.

This model neglects effects due to interactions between molecules, which is difficult to estimate without a proper theory for liquid structures. However, it gives an order-of-magnitude estimate for the zeroth and the first order terms.

We now assume that Δn obeys the following relaxation equation[22]

$$(\frac{\partial}{\partial t} + \frac{1}{\tau})\,\Delta n(t) = \frac{\Delta n_o(|E|^2)}{\tau} \qquad (3)$$

where τ is the relaxation time associated with the randomization of the molecular orientation after the field is shut off, and Δn_o is given by Eq. (2), τ is roughly proportional to the viscosity of the liquid. For CS_2 and toluene, τ is ~ 2 psec and ~ 10 psec respectively. Eqs. (3) and (2) summarize the non-linear properties of the media to be considered.

2. Propagation of Electromagnetic Wave in a Non-Linear Medium

The starting point is the wave equation,

$$\nabla^2 \underset{\sim}{E} - \frac{1}{c^2}\frac{\partial^2}{\partial t^2}\,\underset{\sim}{D} = 0. \qquad (4)$$

In a nonlinear medium described by Eqs. (2) and (3), for a linearly polarized electric field, $D = \varepsilon E = (n_o + \Delta n)^2 E$, the propagation of the electromagnetic wave is described by the set of coupled equation

$$\begin{cases} \nabla^2 E - \frac{1}{c^2}\frac{\partial^2}{\partial t^2}\,[(n_o + \Delta n)^2 E] = 0 \\ (\frac{\partial}{\partial t} + \frac{1}{\tau})\,\Delta n(t) = \frac{\Delta n_o}{\tau}\,. \end{cases} \qquad (5)$$

For an input pulse whose duration is much longer than τ, $\Delta n(t) = \Delta n_o$ and Eq. (5) can be solved in quasi-steady state approximation. Thus, if $E = 1/2(\mathcal{E}(r,z)e^{i(kz-\omega t)} + c.c)$ and neglecting higher order terms which are small, we have, from Eq. (5), in cylindrical coordinates,

$$\frac{\partial^2}{\partial r^2}\,\mathcal{E} + \frac{1}{r}\frac{\partial \mathcal{E}}{\partial r} + 2ik\,\frac{\partial \mathcal{E}}{\partial z} + \frac{\Delta n_o}{n_o}\,k^2 \mathcal{E} = 0 \qquad (6)$$

Two categories of techniques have been used to solve the non-linear equations, namely, numerical solution using computers, and paraxial-ray "constant shape" approximation.

a. Numerical solutions. Numerical technique was first used by Chiao et al.[3] to obtain the precise power and spatial distribution needed for a steady state, self-trapping beam, assuming $\Delta n = n_2|E|^2$. The power for trapping is given by $P_T = 5.763\,\frac{\lambda^2 c}{16\pi^3 n_2}$ and is independent of the size of the beam. Self-trapped solution with all orders of the Δn expansion used[13] were also obtained later.

Self-focusing solution was obtained by Kelley[4] through solving Eq. (6) numerically, assuming $P \sim 300\,P_T$. From this numerical solution and other physical reasoning, he obtained an approximate equation for self-focusing length Z_f (defined as the distance at which the intensity at the axis increases substantially) as a function of input power, P

$$z_f = K/(\sqrt{P} - \sqrt{P_{cr}}) \tag{7a}$$

$$K = \left(\frac{n_o}{4}\right)(a^2)\left(\frac{c}{n_2}\right)^{1/2} \tag{7b}$$

$$P_{cr} = \frac{(1.22\lambda)^2 c}{256\, n_2} \tag{7c}$$

where a is the beam radius and P_{cr} has the physical meaning that the input beam will diffract if $P < P_{cr}$, self-traps if $P = P_{cr}$, and self-focuses if $P > P_{cr}$. [The discrepancy between P_T and P_{cr}, which is about $P_T/2$, is due to the somewhat arbitrary physical reasoning used by Kelley[4] to obtain P_{cr} (see the following paragraph)].

Subsequent numerical solutions of Eq. (6) by Dawes and Marburger, and Goldberg et al.[15] using a wide range of values of input power P below and above the threshold showed that for $P > 1.5\ P_T$

$$z'_f = K'/(\sqrt{P} - 0.858\sqrt{P_{cr}}) \tag{8a}$$

$$K' = 0.369\, ka^2 P_{cr}^{1/2} = 0.25 n_o a^2 \left(\frac{c}{n_2}\right)^{1/2} = K' \tag{8b}$$

$$P'_{cr} \simeq P_T = 5.763\, \frac{\lambda^2 c}{16\pi^3 n_2} \tag{8c}$$

which are quite close to the approximate expressions of Kelley. These expressions are for input beam with Gaussian spatial distribution. For non-Gaussian smooth input beam, it was found numerically that K' can be replaced by K'/f for $P \gg P_{cr}$ where f is of the order of 1. The parameter f was first introduced by Wang,[3] whose experimental results agreed with these predictions. The value of P'_{cr} with $f \neq 1$ also increases as f increases.

Dyshko, et al.[17] also solved Eq. (6) numerically, using a Gaussian input beam. The numerical computing scheme used was different from that used by Kelley,[4] Dawes, et al., and Goldberg et al.[15] The critical power P_{cr} for self-trapping obtained agrees well with the value P_T of Chiao, et al.[3] and Dawes et al.[15] For $P > P_{cr}$, a finite set of intensity maxima were found along the axis, the number of which increased (at $P \gtrsim P_{cr}$, only one maximum exists) as P increased. The first maximum (the one with shortest focal distance) appears to coincide with that calculated by Kelley,[4] Dawes et al., and Goldberg et al.[15] No analytic relations known were given for z_f vs P.

Fleck and Kelley[24] solved the time-dependent coupled Eq. (5) numerically for $P = 12.5\ P_T$ for various pulse widths δt of the order of the relaxation time τ. They found that even for $\delta t/\tau = .475$, self-focusing still occurs; however, the focusing distance is about four times that of $\delta t/\tau = \infty$.

b. Calculations using the paraxial ray approximation. This method was first employed by Talanov[2,5] to obtain self-trapping and self-focusing solutions. It was also used by Akhmanov, et al.,[6] Wagner, et al.,[14] and Wang.[23] The analytic solutions obtained in this approximation were found to be in good agreement with results from numerical solutions of the nonlinear equation.

Expressions from this approximation corresponding to Eq. (7) and Eq. (8) are[14]

$$z_f = K''/((P - P''_{cr})^{1/2} - a_o\, k \tan\theta_o) \qquad (9a)$$

$$K'' = (P''_{cr})^{1/2}\, k\, a_o^2 = 0.52\, ka^2 P_T^{1/2} \simeq 1.4K \qquad (9b)$$

$$P''_{cr} = \lambda^2 c/(32\pi^2 n_2) = 0.273\, P_T \qquad (9c)$$

where a_o is the initial radius of the beam and θ_o is the initial divergent angle of the beam. This set of expressions is quite close to that of Eq. (7) and (8). The size of the beam a as a function of propagation distance z, at any input power P is given by

$$a = \left[\left(1 - \frac{P}{P''_{cr}}\right)\frac{z^2}{k^2 a_o^4} + \left(1 + \tan\theta_o \frac{z}{a_o}\right)^2\right]^{1/2} \times a_o. \qquad (10)$$

Eq. (10) should be a good approximation so long as the constant-shape approximation assumed in this method is not drastically violated.

From these calculations, we can summarize by the following: (a) steady state self-trapped solutions exist. They require the total power be precisely equal to certain values of P_{cr} which depend on the input intensity and spatial distribution. For $\Delta n = n_2|E|^2$ the self-trapping power is independent of the beam size (for a fixed spatial distribution). (b) When the input power is higher than the self-trapping power a number of intensity maxima occur along the axis. The location of the first maximum (with the shortest focal distance)[45] as a function of input power can be approximately given by an expression of the form

$$z_f = K_e/(\sqrt{P} - \sqrt{(P_{cr})_e}) \qquad (11)$$

where the exact values of K_e and $(P_{cr})_e$ depend on the detail input intensity distribution. Rough estimates and functional dependence of K_e and $(P_{cr})_e$ can be obtained from Eqs. (7), (8), or (9). The exact values can be obtained most conveniently by experiments similar to that of Wang.[8] In the remaining part of this work, we will drop the subscript, e, remembering that K and P_{cr} are obtained experimentally rather than from the expressions (7), (8), or (9).

B. Model of Filaments

In this section we shall describe the proposed models for filaments. We shall examine how successful they are in explaining the observed facts about filaments mentioned in Section I. Theses include:[10-12] (1) the appearance of dots of roughly constant size in the end view picture taken at various cell lengths, (2) the characteristic sizes of this dot for different liquid media, (3) the duration of the filament, (4) observation of thin streaks from the side view, and (5) the energy content of the filament of the order of a few ergs in CS_2 and in toluene.

1. Model of Self-Trapped Filaments (STF)

This model was first proposed by Brewer, et al.[12] In this model, the filament is pictured as a self-maintaining waveguide of constant diameter satisfying the conditions for the self-trapping solution of the non-linear equations described earlier.

It is obvious that this model can explain properties (1) and (4) listed above. For property (2), the characteristic sizes for different liquids were not explained in this model. For (3), it was believed[12] that the destruction of filament after about 10^{-10} seconds results from heating, possibly from the vibrational energy given to the molecules through the stimulated Raman effect converted into vibrational

energy. Heating gives rise to expansion and decrease of refractive index and hence destruction of filament. The time required for this destruction process was estimated to be about 1 nsec, somewhat longer than the experimental value of 0.1 nsec. As for (5), the self-trapping solution requires the power content of a self-trapped beam to be P_{cr}, given by Eq. (8c). The predicted value of P_{cr} is about 10 kw, which roughly agrees with the measured power energy of a few ergs divided by the pulse width of ~ 0.1 nsec of the filament.

The first question concerns the establishment of these self-trapped waveguides. Experiments[10,11] clearly indicated that filaments appeared after the laser beam has self-focused. On the other hand, calculations outlined above show that, for $\Delta n = n_2|E|^2$, if the laser beam initially has a power level higher than P_{cr} to start self-focusing, the self-focused beam will not stabilize into the self-trapping mode. In order to attain an approximately trapped solution (beam diameter oscillating between maximum and minimum) with an initial condition of $P > P_{cr}$, saturation of the nonlinear refractive index is required (i.e., including the higher-order terms in the Δn_o expansion of Eq. (1)). Using the value of Δn_o in Eq. (2), the predicted beam diameter of a self-trapped filament at the saturation region is less than the wavelength of light,[13-15] compared with the observed diameter of a few microns. Further, the predicted power and index change is several orders of magnitude higher than the observed values.[18,30]

If one concludes that the field in the filament is not in the saturation region, the more serious question of stability of the self-trapped solution arises. The self-trapped solution with $\Delta n_o = n_2|E|^2$ requires that the total power equals to P_{cr} precisely for a given spatial distribution. We can see the critical requirement

on power from the following estimate. Suppose we have a beam of 5 microns in diameter initially in the self-trapping mode. Let us see what happens if it suffers a loss of power, whatever the cause might be, of 1% at some point $z = z_o$. Using Eq. (10) we can estimate the diameter of the beam at z = 1 cm, assuming no external power being fed in:

$$d = d_o x \sqrt{(1 - \frac{P}{P_{cr}}) \frac{16z^2}{k^2 d_o^4} + 1} \approx 800\mu$$

where $d_o = 5\mu$, $k = 10^5$ cm^{-1}, z = 1cm, and $P = .99\ P_{cr}$, $\theta_o = 0$. On the other hand, if $P = 1.01\ P_{cr}$, i.e. 1% above the required power, the diameter of the beam would reduce to half the size in a distance of .05 cm. This instability can also be deduced from numerical solutions (see, for example, Fig. 1 of Dawes and Marburger[15]). Experiments indicated that energy does leak out of the filament to make it possible to obtain side-view pictures.[7,11] While it is possible that external power be fed into the waveguide, it seems very unlikely that no more and no less than the exact amount needed be transferred in all the time to maintain such a fine balance.

Due to these questions, alternative models have been proposed.[25] Among them is the model of moving focal spots, which we shall describe next. We shall see later that this model, rather than the self-trapping model, is the more appropriate description of filaments.

2. Model of Moving Focal Spots (MFS).

This model was first proposed by Lugovoi and Prokhorov,[17] who pointed out that in all of the experiments where filaments have been observed, pulsed lasers were used. Due to the time variation of the input power, according to Eq. (11), the self-focusing distance, or

the position of the focal spot, will also vary with time. This focal spot motion along the axis, could account for the observed filaments.

Let us see how the properties of filaments listed before can be explained by this model. Property (1) is correctly predicted. From Eq. (11), we see that if the incoming pulse has peak power $P_{max} > P_{cr}$; for any cell length longer than the minimum length of $z_{min} = K/(\sqrt{P}_{max} - \sqrt{P_{cr}})$, a focal spot will appear at that focusing length. This focal spot is the dot seen at end view pictures taken at various cell lengths. Property (4) is also accounted for since on a time-integrated side view picture, the moving focal spot will appear as a thin streak. For property (5), we expect the power of the focal spot to be slightly higher than P_{cr}. This agrees with the observed result within the experimental uncertainty. For property (3), the duration of the observed filament pulse should equal to the duration, with which the focal spot sweeps through the exit plane of the cell. We shall see later (Section III) that the experimental results agree with the theoretical predictions. Finally, for property (2), the characteristic size of the filament should be simply the size of the focal spot. However, no theoretical calculation on self-focusing has been extended to the focal region to yield the dimensions of the focal spot. Thus, we see that this model is qualitatively superior to the trapping model, at least for the case of nanosecond input laser pulses we are here interested in.

Let us develop the moving focal spot model (MFS) further to see how the focal spot moves in time for a given input pulse.[26,27] In Fig. 1 we plot in the lower trace the incoming power vs time, and in the upper trace the focal spot position vs time. At time, t_A,

the beam with power P_A enters the cell at z = 0. It then travels at velocity of light in the medium indicated by the dotted line, until it reaches the self-focusing distance determined from Eq. (11). At an earlier time, the laser power is lower. Because of the lower power, the light now self-focuses at a larger distance. Thus, point by point, we can plot out the entire curve of the focal-spot trajectory. Here, we have used the steady state expression for the focal distance as a function of power. For input pulses with nanosecond duration, this should be an excellent approximation since typical relaxation time for orientational Kerr effect, which is the dominant mechanism for nanosecond input pulse, is of the order of 10 picoseconds. We should emphasize that, in this construction, the quantities P(t), P_{cr} and K can all be obtained experimentally. The parameters P_{cr} and K can be determined experimentally by measuring the self-focusing threshold as a function of cell length. Once these are determined, and P(t) monitored on the oscilloscope (in terms of P_{cr}, since absolute values are not necessary), the focal spot motion in time and space is uniquely defined.

This curve has many interesting features. If the cell length is less than z_D but larger than the minimum focal distance z_B, the focal spot will first appear at the end of the cell moving inward toward the laser until it reaches the point B. It then moves out again. The turning point B corresponds to the peak of the input pulse. If the cell length is longer than z_D, the focal spot will first appear somewhere inside the cell (at point D), and then immediately splits into two branches, one moving inward toward the laser initially and then away from it (branch DBC), the other branch moving forward all the time (DAE). Since this is a plot of position vs time, the slope

of the curve indicates the "velocity" of the focal spot, which is plotted in Fig. 2 as a function of z_f and t. For example, the region around B has slope close to zero, which means that the focal spot moves very slowly as it turns around. Consequently, if the cell length is close to z_B, the filament pulse emitted at the exit end should become correspondingly longer. Another striking feature is that the velocity of the focal spot along the curve DAE is always larger than the light velocity in the medium. This, of course, does not violate the principle of relativity since this is simply a sequence of focal spots forming at different times and at different places. We shall see that experiments confirmed these predictions and showed clearly that filaments are moving focal spots. Other properties derived from this curve will be discussed in later sections.

From the discussion above, we see that the MFS model is far more definite than the STF model. Quantitative comparisons with experiments are possible for the MFS model once the input conditions are known; while for the STF model, since we do not know how the filament is established, predictions tend to be at best qualitative. The uncertainties in the model itself coupled with the largely unknown effects of the stimulated processes, which we will discuss next, very often makes it impossible to deduce even qualitative predictions from the STF model.

C. Effects of Stimulated Processes

In our discussion of self-focusing and the two models for filaments, we have assumed that the intensity-dependent nonlinear refractive index is the only relevant nonlinearity in the problem. This might be justified in the initial stage of self-focusing where the intensity of the laser beam is low. But in the high intensity region of the focal

spot or in the filament, many nonlinear processes, especially the stimulated scattering processes, are induced, and they can affect strongly the appearance of the filament.[17,26,28,29] What is observed experimentally is therefore the result of a coupling of all the interacting nonlinear effects. The proper model for filament should include all these effects. This clearly is an extremely difficult, if not impossible, theoretical task.[15]

In the absence of a complete model, to gain understanding of the problem, the approach we took was to rely on our physical judgment to see in what ways the models could be implemented in the presence of other nonlinear processes. Whether the physical judgments are appropriate and the deductions are correct can then be checked by proper experiments. More of these will be discussed in the experimental section later.

Although the detail interaction between the many nonlinear processes is very complicated, nevertheless, by keeping track of the space-time causality relations between these processes, we can make certain predictions for the MFS model.[21] The moving focal spots generate, among other effects, stimulated Raman and Brillouin scattering processes. These frequency shifted light signals can propagate in either the forward or backward directions, at velocity of light in the medium. The forward propagating signal affects only the portion of the laser pulse that generates it and propagates together with it. On the other hand, the backward signal sees the entire later part of the incoming laser pulse and gets amplified at its expense, as has been confirmed by experiments.[28] The question we wish to answer is to what extent the focal spot motion will be changed as a result of laser depletion by stimulated processes. In Fig. 3 the focal spot

motion curve is shown; the dotted lines have slope $-C/n_o$ indicating the paths of the focusing laser beam and the backward stimulated radiation which originates from the points where the dotted lines meet the focal spot motion curve. The point A, where the instantaneous velocity of the focal spot is $-C'/n_o$, separates the curve into two parts. For the upper portion of the curve (ABC), the incoming laser power does not see any backward going stimulated signal before focusing into a spot (the forward light path does not intersect any backward light paths). For this portion of the curve, the self-focusing process should not be affected by the backward stimulated processes. Stimulated radiation in the forward direction will deplete power from the self-focused laser beam only near the focal region where the beam intensity is high. Therefore, it will not affect the position of the focal spot significantly, although it could be the cause for the limiting size of the focal spot. We can then conclude that the portion of focal spot motion curve ABC should not be affected much by the stimulated processes, and can be calculated as if they were not present. This is a very important conclusion and is the reason why quantitative comparison with experiment is possible even though we do not understand completely how the stimulated processes affect the filament formation.

For the lower portion of the curve (ADE), the situation is quite different. The incoming laser light, before reaching the self-focusing distance, is intercepted by the backward propagating stimulated signals generated earlier by the preceding focal spots. It is well known, both theoretically and experimentally,[28] that the backward propagating signal will grow at the expense of the incoming laser light. This exponential growth of the stimulated scattering processes eventually

depletes the incoming laser power to such an extent that the self-focusing process is terminated. Based on this, we should expect the focal spot motion curve to terminate not much further than the point A.

These predictions are in agreement with experiment as we shall see later.

If we now consider the STF model in the presence of stimulated processes, the most natural question one would ask is why the Raman gain is so low in the filament. For a self-trapped filament with peak power of tens of GW/cm^2, its power should be depleted by Raman scattering in less than a few millimeters. Thus, little laser light should be seen at the end of a trapped filament of 1 cm long contrary to what is observed experimentally. It was suggested that the answer to this question was in the frequency spreading of radiation in the filament. This broadening effect makes the intensity per frequency bandwidth sufficiently small that the Raman gain is appreciably reduced. Let us now discuss the frequency broadening effect using these two different models and see which one is more appropriate.

D. Frequency Broadening of Light in the Filament

Frequency broadening of light in the filament is another nonlinear effect observed in connection with the filament. Light emerging from the filament was shown to be broadened hundreds to thousands of wave numbers.[31] Although frequency broadening would not affect either self-focusing or self-trapping, it is important in helping the understanding of filaments. Frequency broadening is one of the very few observed facts people used as evidence for the existence of self-trapped filaments. For this reason, we will discuss this in some detail.

Frequency broadening of light arises because the light is phase modulated in time.[31] If a light wave $E(t)e^{-i\omega_o t}$ propagates through a slab of material with a refractive index $n_o + \Delta n(z,t)$, the phase increment acquired due to the induced $\Delta n(z,t)$ is given by

$$\Delta\phi(t) = \frac{\omega_o}{c}\int_{z_1}^{z_2}\Delta n(z,t)dz \tag{12}$$

where the integration is along a light path from z_1 to z_2. If Δn varies with time or the path length changes with time, $\Delta\phi$ would also vary with time. The spectrum of such a phase-modulated light wave is given by its Fourier transform

$$E(\omega) = \frac{1}{\sqrt{2\pi}}\int_{-\infty}^{\infty}E(t)e^{-i\omega_o t}\,e^{i\Delta\phi}e^{i\omega t}dt =$$

$$= \frac{1}{\sqrt{2\pi}}\int_{-\infty}^{\infty}E(t)\,e^{i(\Delta\omega t+\Delta\phi)}dt \tag{13}$$

where $\Delta\omega = \omega-\omega_o$.

If the amplitude variation of $E(t)$ with time is sufficiently slow, then the maximum frequency shift can be approximated by the expression

$$|\Delta\omega|_{max} \sim \left|\frac{\partial\Delta\phi}{\partial t}\right|_{max}. \tag{14}$$

Let us now apply this to the problem of filament. We first consider calculations based on the STF model. Two closely related calculations have been given, namely, that of Cheung, et al.[32] and that of Shimizu[31] and Gustafson et al.[33] In both calculations, the length of the filament (the region where Δn is non-zero) is assumed to be constant, independent of time. From Eq. (12) we thus have,

$$\Delta\phi(t) \quad \frac{\omega_o}{c}\Delta n(t)\ell \tag{15a}$$

and hence

$$|\Delta\omega|_{max} \sim \frac{\omega_o}{c}\left|\frac{\partial\Delta n(t)}{\partial t}\right|_{max}\ell \tag{15b}$$

where ℓ is the length of the filament. The time variation of $\Delta\phi$ comes from the explicit time dependence of $\Delta n(t)$ only. In the calculation by Cheung et al., it was assumed that the initial optical field contains two frequency components, one at the input laser frequency, ω_o, and the other at $\omega_1 = \omega_o + \omega_S$, the origin of which was not understood. The amplitudes of these electric field components were assumed to be constant in time, but the beating between the two frequencies ω_o and ω_1 will modulate the index of refraction Δn at a frequency ω_S which gives the time varying $\Delta\phi(t)$. For the calculation by Gustafson et al., instead of assuming the additional frequency component, it was assumed that the filament (and thus the region of non-zero Δn) has a short duration, τ_p and that

$$\Delta n = n_2|E|^2(t)$$

or for medium with finite relaxation time τ for the refractive index change

$$\Delta n(t) = \frac{1}{\tau}\int_{-\infty}^{t} n_2|E(t')|^2 \quad e^{-(t-t')/\tau}\,dt'.$$

This time dependence of Δn which exists for a duration of the order of $\tau_p + \tau$, yields the phase modulation $\Delta\phi(t)$. Note that the assumption of a short pulse duration τ_p gives a band of frequencies extending to $\omega_o \pm 1/\tau_p$. Therefore, when $1/\tau_p$ is chosen to be ω_S the spectra

predicted by these two calculations are very similar, as shown in Fig. 4 together with the experimental spectrum. Typical values of ω_S and τ_p are a few cm^{-1} and a few psec, respectively.

The agreement between the theoretical calculations and the experimental results on frequency broadening[32-34] was used as the proof that the observed filaments are indeed the self-trapped filaments. Based on the extent of the frequency shift observed, it was also concluded that the filament observed can be trapped for centimeters.[18]

However, we shall now show that by extending the MFS model to include the finite relaxation time of Δn, we can also obtain frequency broadening for light emitted from the filament under appropriate conditions. Depending on the input conditions, the extent of frequency broadening varies. The theoretical calculations appear to have semi-quantitative agreement with the observed results. Let us first present a qualitative picture of our theory. If an intense focal spot moves in a nonlinear medium, it should leave behind it a track of field-induced refractive index, Δn, which lasts at least over a period of the order of the relaxation time τ for the refractive index change. We can therefore picture that there is a leaky optical waveguide of finite length moving along with the focal spot. Part of the self-focused light then gets trapped temporarily in this waveguide. If the focal spot is moving in the forward direction with a velocity close to the velocity of light, then the trapped light can remain trapped over a long distance until it runs out of step with the moving waveguide. As a result of the induced Δn, the self-focused light traversing the medium acquires an increment of phase $\Delta\phi$. Since the focal spot moves with time, $\Delta\phi$ appears as a function of time t. A rapid phase modulation $\Delta\phi(t)$ would then lead to a broadened spectrum.[31]

This would happen if, towards the end of the nonlinear medium, the focal spot moved with a velocity close to the light velocity.

From our earlier discussion, we see that we can use the stationary theory of self-focusing to calculate the position and velocity of the focal spot, as shown in Figs. 1 and 2. We see that if the variation of P(t) with t is sufficiently fast, then the focal spot will indeed move with a velocity close to the light velocity c'. This situation is most easily realized from short input pulses.

As to the variations of $|\vec{E}(r,t)|^2$ and $\Delta n(\vec{r},t)$ in the focal region, one must solve for the detailed self-focusing dynamics. In particular, even though the stationary theory of large-scale self-focusing predicts the position of the focal spot fairly well for a long input pulse, it would not describe correctly $|E(\vec{r},t)|^2$ in the small-scale focal region since here, Δn is not likely to respond instantaneously to the variation of $|E(\vec{r},t)|^2$ as a result of the focal-spot motion. The transient response of Δn, together with diffraction and various types of losses, would make self-focusing of the beam more gradual in the focal region, and eventually overcome by diffraction. However, for our qualitative discussion later, an exact solution of $|E(\vec{r},t)|^2$ will not be necessary. Let us consider for the moment self-focusing of the leading part of the pulse (as discussed in the last section, due to backward stimulated radiation, the trailing part of input power is depleted and will not self-focus), and consider only $|E(z,t)|^2$ around the focusing axis. We simply assume that as a beam self-focuses, $|E(z,t)|^2$ increases linearly in the pre-focal region over a distance a, remains constant over the longitudinal dimension 2b of the focal spot, and then as a result of partial trapping or nonlinear diffraction, decreases slowly and exponentially to zero. Then, at a fixed z, if we neglect the small

curvature of the U curve around z in Fig. 1, we would have

$$|E(z,t)|^2 = A[t-(t_z-T_1-T_2)] \quad \text{for } t_z-(T_1+T_2) < t < t_z - T_2$$

$$= AT_1 \quad \text{for } t_z - T_2 < t < t_z + T_2$$

$$= AT_1 \exp[-(t-t_z-T_2)/\tau'] \quad \text{for } t > t_z + T_2$$

with

$$A = 16\, P/cd^2\, T_1$$

$$T_1 = a(v-c')/vc' \qquad (16)$$

$$T_2 = b(v-c')/vc'$$

where t_z is the time when the focal spot appears at z, P is the input laser power at $(t_z - z/c')$, d is the diameter of the focal spot, and v is the velocity of the focal spot at z. As one would expect, the parameters a, b, and d should generally depend on P(t), the diameter, and the spatial distribution of the input beam, and on the properties of the medium.

We should emphasize that Eq. (16) is only meant to be a crude approximation of the true pulse. However, our qualitative discussion below will not be affected by the detailed pulse shape as we shall see. There is some arbitrariness in choosing the values for T_1 and T_2 (or a and b), but in ordinary liquids $(T_1 + T_2)$ must be of the order of the relaxation time τ (~ a few psec. for orientational relaxation) for Δn. (Correct value of T_1 and T_2 can be obtained only by solving the detailed self-focusing dynamics.) It cannot be much smaller since, from experimental observations,[12,30] we know that the maximum $\Delta n(t)$ at z

on the axis is not much less than $\Delta n_o(z) - (1/2)\, n_2 |E(z,t)|^2_{max}$. The value of $(T_1 + T_2)$ cannot be much larger either since, if $(T_1 + T_2) \gg \tau$, we would expect the stationary self-focusing theory to be valid even in the focal region, but we know that when the stationary self-focusing theory holds the focal spots would be sharp with $(T_1 + T_2) < \tau$,[4,24] contradictory to the original assumption. Also, we noticed in our experiments[26] that the focal spots are usually well defined, suggesting that $(T_1 + T_2)$ cannot be much larger than τ. There is also arbitrariness in choosing a value for τ' in Eq. (16). A larger τ' corresponds to trapping of light over a longer duration. Self-trapping of light (i.e., trapping of light by its own instantaneous power in a nonlinear medium)[3] occurs as τ' becomes infinite.

We now assume that Δn obeys the simple relaxation equation

$$\partial(\Delta n)/\partial t + \Delta n/\tau = (n_2/\tau)\, |E(t)|^2 \qquad (17)$$

where n_2 is the nonlinear refractive index. With $|E(z,t)|^2$ given by Eq. (16) we can then solve for $\Delta n(z,t)$ around the focusing axis. Let us again refer back to Fig. 1. Consider the laser light entering the medium at t_A and propagating in the medium along AA' in Fig. 1. Because of the induced Δn, the part of the self-focused light which trails the moving focal spot along the axis acquires a phase increment $\Delta\phi$ at $z = \ell$ given by

$$\Delta\phi(t=t_A+\ell/c') = \int_o^{\ell} (\omega/c)\Delta n(z,t'=t_A+z/c')dz. \qquad (18)$$

From the Fourier transform of $P_f^{1/2} \exp[-i\omega t + i\Delta\phi]$, where $P_f = (d^2c/16)\, E(\ell),t^2$, we can obtain the power spectrum of the light pulse emitted from the small-scale filament at the end of the medium.

As an example, we consider the case of propagating the 1-nsec laser pulse of Fig. 1 into a CS_2 cell 22.5 cm. long. We assume $T_1 = 1.5\tau$ (a = 0.50 cm.), $T_2 = 0.15\tau$ (b = 0.05 cm.), d = 5 μm, $n_2 = 10^{-11}$esμ, $\tau = 2 \times 10^{-12}$ sec., and $\tau' = 3 \times 10^{-12}$ sec. In Figs. 5a and 5b we have plotted $P_f(t)$, and $\Delta\phi(t)$ as functions of t, and in Fig. 5c, the corresponding power spectrum. It is seen that the output filament pulse is about 4 psec. long, and its power spectrum has the characteristic spectral broadening and semi-periodic structure observed in experiments.[31-33] The asymmetry of the $\phi(t)$ curve is reflected by the Stokes-anti-Stokes asymmetry in the spectrum. Such a spectral broadening was earlier explained by assuming the existence of a self-trapped filament with a certain definite length.[31-33] It is interesting to note that in order to explain the observed spectral broadening in CS_2 using the self-trapping model, Gustafson et al.[33] had to assume a filament pulse with a pulsewidth of a few psec., which is about equal to the filament pulsewidth we obtained from our calculation. To see the effect of partial trapping on spectral broadening, we show in Figs. 6 and 7 the broadened spectra corresponding to $\tau' = 3\tau$ and $\tau' = 5\tau$ respectively, with all the other parameters kept unchanged. We also show in Fig. 8 the spectrum for the special case where we assume no trapping at all. (The corresponding filament pulse has the exponential decay replaced by $A[T_1 - (t-t_z-T_2)]$). It is seen that trapping affects only the detailed structure of the broadened spectrum, but it does not change appreciably the extent of spectral broadening on the Stokes side. In particular,

with no trapping (Fig. 8), the semi-periodic structure in the broadened spectrum is largely smeared out. On the anti-Stokes side, however, there is more broadening if the trapping duration is longer. We have also tried other values of T_1 and T_2. Qualitatively, the phase modulation is stronger for larger values of T_1 and T_2 and, hence, the spectrum shows more broadening.

In fact, the extent of spectral broadening on the Stokes side is given approximately by $\Delta\omega_{max} \approx -(\partial\Delta\phi/\partial t)_{max}$, when the inverse of the duration of the filament pulse is small compared with $\Delta\omega_{max}$. To find $(\partial\Delta\phi/\partial t)_{max}$ at $z = \ell$, we can approximate the upper branch of the U curve in Fig. 1 by a straight line in the range of interest. Then, the light propagating along AA' in Fig. 1 reaches $z = \ell$ at the time $t = t_\ell + (\ell - z_A)(1/c' - 1/v)$ where t_ℓ is the time when the center of the focal spot appears at $z = \ell$. From Eq. (18) we now have

$$(\partial\Delta\phi/\partial t)_{z=\ell} = (1/c' - 1/v)^{-1} (\partial/\partial z_A) \int_{z_A-(a+b)}^{\ell} (\omega/c)\Delta n(z,z_A)dz \quad (19)$$

where the integration is along the path AA'. Since the input laser power is essentially constant for the small duration of the filament pulse, Δn is essentially independent of z_A. We then have

$$\begin{aligned} \Delta\omega_{max} &\approx -[(\partial\Delta\phi/\partial t)_{z=\ell}]_{max} \\ &= (1/c - 1/v)^{-1}(\omega/c)\ (\Delta n_{max})_{z=\ell}. \end{aligned} \quad (20)$$

In Eq. (20), $(\Delta n_{max})_{z=\ell}$ is the only quantity which depends on the detailed self-focusing dynamics, but as we mentioned earlier, $(\Delta n_{max})_{z=\ell}$ should not be much less than $\Delta n_o = (1/2)n_2|E(\ell,t)|^2_{max}$ which can be estimated from measurements.[12,30] Spectral broadening should become more appreciable when, towards the end of the medium, the velocity v of the focal spot approaches the light velocity c'. For $\Delta n_{max} \sim 10^{-3}$, $v = 1.01\ c'$, we would have $(\Delta\omega_{max}/\omega) \sim 0.1$. The above approximation breaks down if the curvature of the U curve becomes important in calculating $\partial\Delta\phi/\partial t$. This happens only when the input laser pulse has a pulsewidth comparable with τ. Note that in our case, as a result of focal-spot movement, spectral broadening arises because the length of the optical path in which $\Delta n \neq 0$ varies with time. In the earlier calculations,[9,10] the optical path with $\Delta n \neq 0$ was assumed to have a constant length, and it is through the explicit dependence of Δn on time that spectral broadening comes in.

From the model discussed here, we expect to find small-scale filaments of different characteristics under different experimental conditions. This explains the many different results reported in the literature on the subject. Fig. 1 suggests that, in general, we should expect to see three different types of small-scale filaments depending on the input conditions.

(1) If the length of the medium ℓ (relative to the input laser pulse) is small such that $z_B < \ell < z_D$ in Fig. 1, then the filament is composed of a moving focal spot which moves from the end of the medium inward to z_B and then moves out again, assuming that self-focusing is not affected by stimulated scattering. Little trapping would exist and essentially no spcetral broadening of light emitted from the small-scale filament should be observed.

(2) If $\ell > z_D$, but not excessively large, the focal spot first appears at z_D and subsequently splits into two, one moving forward and the other first moving backward to z_B and then moving out again (see Fig. 1). In this case, since the forward-moving focal spot has a velocity much faster than c', light cannot be trapped over any appreciable distance. The spectrum of the filament pulse emitted at the exit end, would have no appreciable broadening. The spectral width does, however, increase somewhat with the length of the medium. Again, these predictions were confirmed by the experimental results obtained from a single-mode, Q-switched laser.[26] [See Section III(C).]

(3) If $\ell \gg z_c$, so that the velocity of the moving focal spot approaches c' towards the end of the medium, then part of the self-focused light trailing after the focal spot can be trapped over a long distance. The filament pulse emitted from the medium would probably have a duration of the order of τ. Its spectrum should now have appreciable broadening which increases as the length ℓ increases,[18] since the velocity v of the focal spot approaches c' as ℓ increases (see Fig. 2). In usual experiments, with a reasonable length ℓ, this situation is most easily realized by a short input laser pulse. We notice that filaments with large spectral broadening were observed only when a mode-locked laser[19] or a multimode, Q-switched laser[18,32] was used.

III. EXPERIMENTS AND RESULTS

In this chapter, we shall describe the experiments and discuss the results obtained. We divide the experiments into three general groups. The first group is primarily to obtain the properties of filaments under controlled input conditions, the second group to study the relation between filaments and the various stimulated processes, and the third group to investigate which of the two proposed models is the correct one.

We use a water-cooled ruby laser, pumped by a linear flash-lamp in an elliptical cavity. To obtain maximum spatial homogeneity for the output beam, a high quality ruby rod (Union Carbide Select Grade) was used, and a pinhole of about 1 mm diameter was put inside the laser cavity. The laser is Q-switched by cryptocyanine in methanol to yield a smooth pulse with duration about 8 nsec full width at half maximum (FWHM), as measured by a fast photodiode in combination with a Tektronix model 519 oscilloscope (overall time constant is about .4 nsec). The spectral content of the pulse is measured using Fabry-Perot interferometer and is shown to be $\leq .01\ cm^{-1}$. The maximum peak power of the laser beam is about 200kw. A typical laser pulse and its Fabry-Perot pattern are shown in Fig. 9.

When the output of this laser was sent into a liquid cell containing CS_2 or toluene, the advantage of this system compared to a multimode laser is evident. For each laser shot, instead of seeing tens and hundreds of filaments,[10-12] only one filament was observed. It is thus possible to study what is the relation between the input power and the properties of that one filament, rather than the average of many filaments.

A. Experiments to Study the Properties of Filaments Under Controlled Input Conditions

SIZE: The experimental setup is shown in Fig. 10a. Typical lengths of the cell containing the nonlinear medium ranged from 10 cm to 50 cm. To observe the size of the filament, we took magnified (100 ×) pictures of the beam cross section at the exit window of the cell. The film used was either Polaroid Type 47, or Kodak Royal Pan Sheet Film from which densitometer traces can be performed to obtain quantitative measurement of the sizes of the filament.

Fig. 10 shows our experimental results of the beam cross sections at a constant cell length as the input laser power was increased from below to above threshold for self-focusing. Below threshold, [Fig. 10b] the beam cross section was roughly the size of the input beam, in this case ~ 750 μ. As the input power was increased to what we would define as threshold value, a bright spot of about 50 μ in diameter appeared [Fig. 10c]. With further increase of input power, the bright spot shrank to a more or less limiting filament size [Fig. 10d]. Further increase of power above this value did not change the size, but the energy content appeared to decrease. Fig. 10e shows a collection of filaments with this characteristic limiting size.

Similar results were obtained when we kept the input power constant, but gradually increased the cell length. The shrinking of beam cross section to the limiting size was seen. After the limiting size was reached, further increase of cell length did not change the size, but decreased the energy content. When the cell length was much longer than the threshold length (~ 20 cm longer) the dot diffused into the background and became difficult to observe.

For each liquid, there is a characteristic limiting size. Fig. 11 shows a typical densitometer trace of a CS_2 filament. The full width at half maximum (FWHM) was measured to be 5.6 microns for this case. In general, the limiting sizes of filaments measured for CS_2, toluene, and nitrobenzene were 5 ± 1 μ, 10 ± 2μ, and 20 ± 2μ respectively.

This limiting size appeared to be independent of temperature of the liquid. In CS_2, when the temperature of the liquid was raised to 48°C (close to the boiling point), the size of the filament remained unchanged.

In liquid mixtures, the limiting size of the filament smoothly varied from one limit to the other as the mixture content changed from one liquid to the other. Typical result is shown in Fig. 12 for CS_2-nitrobenzene mixture.

DURATION: To measure the duration of the filament, one must somehow block off the unfocused background laser light. This blocking must be carefully done in view of the fact that the energy content of the input laser beam is of the order of 10^4 ergs while the energy content of the filament is of the order of 10 ergs. The property used in differentiating the filament from the background is the large diffracting angle of the filament at the exit window of the cell. A typical setup is shown in Fig. 13(a). Lens L_1 images the end of the cell E to the plane A. A disc D of 1 mm diameter was put in between L_1 and A, slightly beyond the focus f_1 of the lens, to block off the unfocused background laser light emerging from the cell at small divergent angle. The exact position of the disc was adjusted experimentally to allow maximum amount of filament light in while completely blocking the background light. To minimize

scattered laser light by impurities, dust particles, etc., L_2 is used to magnify the image at A so that only a small area around the filament is seen by the detector at plane B. From Fig. 13(b) we see that besides blocking light with small divergent angle, this setup also discriminated against light diverging from deep inside the cell. For a light source at a distance d from the end of the cell emitting light within a cone angle of $\theta_o = 4 \times 10^{-2}$ radian in air (we assume constant light intensity within the cone, and zero intensity outside), the percentage of light signal that will reach a detector of 2.5 cm diameter at B is shown in Fig. 13c. The dotted line represents the case when L_2 is taken away and the detector is placed at the plane A. We thus see that with the two-lens system, the detector would only see light diverging from within a few centimeters from the end of the cell.

Fig. 14 shows a typical set of data for a constant cell length, as the input power was increased from below to above threshold. Below threshold, (Fig. 14a) the laser beam was completely blocked by the disc. When the input power reached threshold, a pulse of 1 nsec or longer appeared (Fig. 14b). For higher power, the filament pulse duration decreased to about .5 nsec; and eventually down to less than .1 nsec (Fig. 14c,d).

For pulse width less than .5 nsec, it was necessary to use the convolution technique to deduce the true pulse duration. The essence of the technique is to extract the pulse signal S(t) from the convolution integral $R(t) = \int_{-\infty}^{t} S(\tau)\, g(t-\tau)\, d\tau$ where R(t) and g(t) are the observed pulse from the detection system and the response function to a δ function (approximated by a mode-locked laser pulse of about 10 psec as measured by two-photon fluorescence measurement),

respectively. Allowing the possibility of different pulse shapes, we were able to measure the pulse width with an accuracy of ± 30 psec for a 200 psec pulse and of ± 60 psec for a 100 psec pulse. In Fig. 15 we show the functions g (t), R(t) and S(t) for two different pulses. For a rough estimate of the pulse width, we note that if the oscilloscope trace returns closer to the base line after the first peak, then the pulse duration is correspondingly shorter. This technique has a practical limit of about 100 psec, below which we cannot resolve. Other techniques commonly used for picosecond measurements, such as two photon fluorescence and harmonic correlation measurements, either require a large number of identical pulses or an intense beam of fairly large cross section, both of which are not available in the case of filaments.

Simultaneous measurement of size and duration correlated the 50 μ dot with the 1 nsec pulse. When the limiting size was reached, the duration decreased to about 200 psec; and then as the size remained unchanged, the pulse duration continued to shorten to less than 100 psec, with the peak power remaining roughly unchanged.

ENERGY AND POWER CONTENT OF THE FILAMENT: The energy of the filament can be measured either by photographic technique or by calibrated photodiode. For a filament that has already reached the limiting size, the peak power was estimated to be about 30 kw for toluene and 8 kw for CS_2. In both cases, within the experimental uncertainty, at the limiting size, the peak power seemed to be independent of the pulse duration. For a 30 kw toluene filament of 10 microns lasting 100 psec, the energy density is about 4 joules/cm^2 while the incoming laser energy density (with an 8 nsec pulse width) is about .4 joules/cm^2. Thus, the filament can show up clearly on time-integrated pictures.

SIDE VIEW OF THE FILAMENT: Side view picture of the filament has been obtained by Brewer and Lifsitz,[11] and Brewer and Townes.[40]

Our attempt to see this was not successful. The cause of this could be due to either mis-focusing or optical setup (we had only one filament to focus on) or that the side scattering of the filament observed by Brewer et al. was not present in our case.

These results showed several points. First, our data on various filament properties (after the limiting size has been reached) largely confirmed the earlier results measured with multi-mode lasers.[10-12] This is important because it showed that, although the input conditions might be quite different, the filament we were studying was the same as the filaments observed by other workers. The fact that tens and hundreds of filaments per shot observed earlier[10] must be the consequence of inhomogeneity and hot spots in the input beam, rather than an intrinsic property of the filament.

Second, from the consistency of our experimental data from shot to shot, and the fact that only one filament appeared per shot, we see the possibility to compare in a quantitative manner with the predictions of the model, especially the MFS model.

Third, we see that, although for each liquid there exists a limiting size for the filament, yet before this is reached, there is a regime where the duration and the size is dependent on the input power. For the size variation, the analysis of Maier, Wendl, and Kaiser[29] showed that the phenomenon can be described very well by the steady-state self-focusing theory. For the change in duration of the filament as a function of input power, the observed result agreed with the prediction of the MFS model. Below threshold for

self-focusing, the entire beam should be blocked by the disc, as seen in Fig. 4a. At threshold power, the turning point of the focal spot motion curve (Fig. 1) is close to the end of the cell. Since the detector collects light emitted from a few cm region near the end of the cell, we expect to see a long pulse, as predicted from Fig. 16 (curve for P_1). At higher input power, the time that the focal spot spends in the few cm region monitored by the detector decreases correspondingly (curve for P_2), and therefore we should expect the duration of the filament pulse to decrease, in agreement with the experimental data (Fig. 14c,d).

The observation of only one short pulse (corresponding to one focal spot) is consistent with the theoretical calculation of Dyshko et al.[17] For our laser power $P \sim 3\ P_{cr}$, a beam radius a of 250 μ, and cell length ℓ of 32.5 cm, the parameters $\xi = \frac{\ell}{ka^2} \simeq 0.5$, and $N \simeq 2(P/P_{cr})^{1/2} \simeq 3.5$, and the predicted number of focal spots is one [see Fig. 2 of Abramov et al.].[27]

This set of experimental results gave the first indication that the MFS model is correct.

B. Experiments to Study the Correlations Between Filaments and Stimulated Scattering Processes

1. Since stimulated scattering processes always appear together with fialments, it is helpful to know as much as we can about these scattering processes in connection with the filament formation. In this experiment, we simultaneously monitor the incoming light pulse, the pulse emitted from the filament at the end of the cell, the forward Raman pulse, the backward Raman pulse, the backward Brillouin pulse, and the filament picture. The experimental setup is shown in Fig. 17. The liquid used in this case was toluene.

A typical set of data is shown in Fig. 17. As the input laser pulse increased from below to above threshold, the following sequence of events happened:

(a) Below threshold for self-focusing, no stimulated scattering occurred [Fig. 17a].

(b) When the input power is close to threshold value, the beam cross section shrank to about 50 microns; the filament pulse was about 1 nsec; backward Brillouin scattering was present, but both backward and forward Raman signals were absent [Fig. 17b].

(c) With slightly higher power, the filament size shrank to within a factor of 2 of the limiting size; the duration of the filament pulse decreased to less than 1 nsec; backward Brillouin light remained unchanged; backward Raman appeared, while forward Raman, though present, was very weak in intensity [Fig. 17c].

(d) With higher power, the size of the filament reached its limiting value; the duration decreased to about 200 psec; forward Raman light increased substantially while backward Raman and Brillouin light remained roughly the same [Fig. 17d].

(e) Further increase of laser power reduced the duration of the filament to less than 100 psec. The size of the filament and the stimulated scattering signal intensities remained roughly unchanged [Fig. 17e].

The typical peak powers of these stimulated processes were 10 kw for backward Brillouin, about 10 kw for forward Raman and about 100 kw for backward Raman, compared to about 30 kw for the filament pulse. The duration of the backward Brillouin pulse was about 1 - 2 nsec, while the duration of the Raman pulses were less than .1 nsec.

These results indicate that the self-focusing process initiates

first the stimulated Brillouin process, and subsequently the stimulated forward and backward Raman scatterings. From the intensity and energy content of the backward Raman and Brillouin processes, we can conclude that the laser power is depleted. This is also shown clearly by the transmitted laser pulse shape, shown in Fig. 18. Similar results in CS_2 have been reported by Maier, et al.[29]

2. In this experiment we measured the time correlation of the filament pulse with the forward and backward Raman pulses to see when and where are these processes initiated. From the above experiments, we know that the duration of these pulses are less than 100 psec. By measuring the time correlations, we can obtain their relative positions to better than 2 cm.

The experimental setup is very simple. The pulses, with known optical or electrical delay, are displayed on a Tektronix Model 519 oscilloscope. The linearity of the sweep rate was calibrated to within 1.5%. Further, the true absolute sweep rate was checked by measuring the velocity of a short light pulse propagating in air. From the oscilloscope trace, the time correlation of the pulses can be easily obtained. (Measurement of the pulse separation on the oscilloscope trace photograph was done using a measuring microscope with an accuracy of ± 1 μ.)

Experimental results showed that the forward Raman pulse is always coincident in time with the laser filament pulse independent of input power level. Simultaneous end view pictures at Raman and laser frequencies showed that spatially the Raman signal appeared as an intense dot at the same position where the laser filament spot is. We can thus conclude that the forward Raman pulse is generated from the filament region.

A more interesting case was the correlation between the backward Raman pulse and the laser filament pulse. In contrast to earlier experimental results,[28] which indicated that the backward Raman light was initiated by the filament at the end of the cell, independent of input condition, we found that the backward Raman pulse was not necessarily initiated at the exit end of the cell and that the time separation between the two pulses was not constant for different input power.

These results are actually natural consequences of the moving focal spot model. Let us again consider the focal spot motion curve. As discussed earlier due to the high intensity, Raman light is generated everywhere along this curve when and where focal spots appear. If all these signals were amplified equally, we would see a long Raman pulse. However, as shown by the calculation of Maier, et al.[28] the leading edge of the Raman pulse is more strongly amplified, since it always sees un-depleted incoming laser light and eventually becomes a short spike, as is observed in experiments. From Fig. 3, since the Raman signal generated at A (where the instantaneous slope is $-c' = -c/n$) precedes Raman signals generated elsewhere, from the argument given above, the backward Raman spike observed in our experiments must originate from the focal spot at A. To see the physical picture of the time correlation between the filament pulse and the backward Raman pulse more clearly, we show in Fig. 19a the experimental setup together with a focal spot motion curve. At t_1, the focal spot at $z_R(t_1)$ (where the instantaneous velocity is $-c/n$) generates the Raman signal, while the forward going focal spot is at $z_F(t_1)$. At t_2, the focal spot reaches the end of the cell ($z_F(t_2)$) and gives the filament pulse while the backward Raman pulse, propagating

at $-c/n$, reaches $z_R(t_2)$. The distance between the Raman pulse and the laser pulse at t_2 is thus $\ell - z_R(t_2) \equiv d$ where ℓ is the length of the cell. Experimentally, knowing the geometry of the experimental setup and the pulse separation in time from the oscilloscope trace, we can trace back and obtain this parameter d. The experimental results for four different cell lengths are shown in Fig. 20, where we plot the parameter d vs input power. Fig. 19b depicts why the pulse separation d should increase with increased input peak power.

To compare these results quantitatively with theoretical prediction, we need to obtain the focal spot motion curve at different power levels corresponding to the actual experimental conditions. To obtain these, we measured the minimum self-focusing distance as a function of the input peak power. This is plotted in Fig. 21. From the slope and the intercept of this curve we obtain K and P_{cr}, from which we can construct the focal spot motion curve using the experimentally measured input power P(t). The theoretical values of d as a function of input peak power at the different cell lengths are plotted as solid lines in Fig. 20. The agreement with experiment is excellent.

This experiment demonstrated that the moving focal spot model is able to predict quantitatively the behavior of the backward Raman spike. It is also an experimental confirmation of the calculation of Maier, et al.[28] Another very interesting point is that it, indirectly, shows that the velocity of the forward moving focal spot is higher than the light velocity in the medium. This conclusion can be arrived at by examining the value of d for the same input power, but at different cell lengths, as follows. In Fig. 22 we show a focal spot motion curve. For a cell length of ℓ_1, the pulse separation d should be d_1. Now for the same focal spot motion curve, if the cell length

is increased by $\Delta\ell$, the additional time it takes for the focal spot to reach the exit window is $\Delta t = \frac{\Delta\ell}{v_f}$ where v_f is the average velocity of the focal spot for that region. During this time, the backward Raman pulse, traveling at light velocity $c' = c/n_o$, would have covered a distance of $\Delta\ell' = \Delta\ell\left(\frac{c'}{v_f}\right)$. If $v_f = c'$, $\Delta\ell' = \Delta\ell$, and the pulse separation d would be increased by $2\Delta\ell$. On the other hand, if $v_f > c'$, $\Delta\ell'$ is less than $\Delta\ell$, and the increase in d would be less than twice the increase in cell length. The theoretical curves in Fig. 20 show that, for the same peak power, the increase in d is always less than twice the increase in cell length, since the forward focal spot always has a velocity higher than light velocity. The agreement between theoretical prediction and experiments thus confirmed this striking feature of the moving focal spot. This property has been measured directly (to be described in the next group of experiments) and is one of the proofs that filaments are moving focal spots.

C. Experiments to Determine the Correct Models

Unless otherwise specified, all of the following experiments were performed using toluene.

1. The most direct and important test for the MFS model is to see experimentally whether the focal spots appear at the predicted time and space according to the focal spot motion curve.

The first indication that focal spots appear as predicted was the observation of a bubble of 100 μ in diameter created at the minimum focal distance.[26] At this distance, the focal spot should stay for a relatively long time, so that there is enough energy to vaporize the liquid. This was observed only when the input peak power was such that the minimum focal distance was close to the end of the cell. For higher power, the backward Raman generated at the focal spot formed

earlier would deplete the input laser light to terminate the focusing action before the turning point was reached. This observation agrees with the theoretical prediction of the MFS model.

To measure the focal spot motion directly, we performed a time-of-flight experiment on the focal spot. Recall that the focal spot velocity has a very wide range of value depending on the region one is looking at. In the region we chose to investigate, the focal spot has a velocity several times the velocity of light according to the MFS model. This region was chosen for two reasons. First, a measured velocity a few times that of light velocity would clearly prove that self-trapping of light cannot be the case. Second, as discussed in the theoretical section, in this region, the self-focusing process is not affected much by the stimulated processes and we can quantitatively compare experimental results with theoretical predictions using the moving focal spot model as if the stimulated processes were absent.

Experimentally, in order to have a focal spot having the desired range of velocity at a reasonable cell length, the diameter of the laser beam was reduced to 300 μ, using an inverted telescope. The maximum peak power of the pulse was about 100 kw. (This corresponds to about 2 P_{cr} for toluene, which was the medium used in this experiment. This power level assured us that for the cell length used, one and only one focal spot would appear.)

As shown in Fig. 23, we used a 36-cm toluene cell, and inserted a beam splitter (a coated microslide of 100 μ thick) a distance d from the end of the cell. Focal spots of about 10 μ in diameter were observed, both at the beam splitter and at the end of the cell. The defocused light from both focal spots was now collected with appropriate

optical delay by the same photodiode and two pulses with duration less than 0.1 nsec showed up on the oscilloscope. The input laser pulse was also monitored simultaneously. With our fast detection system, the time lag Δt between the two short pulses can be measured to within 0.08 nsec. Thus, for d - 6.5 cm and 15 cm, we found Δt = 0.08 nsec and 0.25 nsec, respectively. If the two pulses had come from a short light pulse propagating in a trapped filament, we would have found Δt = 0.32 and 0.75 nsec, respectively. Our experimental results clearly showed that the 10 μ dot seen at various cell lengths was not due to a trapped filament, but due to a focal spot which was moving forward with a velocity faster than the light velocity.

To compare with theoretical predictions, we experimentally determined the parameters K and P_{cr} in Eq. (11), and we monitored the input pulse P(t). The focal spot motion curve can thus be constructed. For the particular input pulse used in the experiment, the focal spot motion curve is shown in Fig. 19 together with the experimental data. It is seen that the measured time delays agree very well with the results obtained from the curve. This is therefore a direct proof of the MFS model.

2. The above experiment clearly demonstrated that focal spots are formed as predicted by the MFS model. We now ask the question: after the focus, would light be trapped?

Early experiments indicated that, after the focal region, light simply diverged. We showed this by focusing the camera system inside the cell rather than at the end of the liquid cell. For a self-trapped filament, we would expect to see a blurred defocused image of the filament dot (see Fig. 24). For a moving focal spot, we should see, instead, a clear dot corresponding to the image of the focal spot

inside the cell. Photographs showed that the focal spot inside the cell did give the expected clear dot. The intensity, however, was less than the dot observed at the end of the cell. This is probably due to depletion by stimulated process in the focal region. The above experiment was performed in the region where the focal spot moves backward.

However, when we tried the same experiment on focal spots that were in the forward moving region, the dot was not observed when focusing inside the cell. There are two possible causes. The self-focused light could be trapped after passing through the focal region. On the other hand, laser light should be converted into Raman light in such a high rate that little is left to be detected on the photograph over the background light.

To see whether light is trapped by the moving focus, we inserted a glass slide (1 mm thick) inside the cell a few millimeters from the exit window. If the filament was trapped, it would be broken up by this piece of glass through diffraction. Thus, the dot appearing at the exit window, if at all, would be much weaker than in the absence of the glass slide, since the energy contained in this dot would only come from focal spots formed after the glass slide. In fact, if without the glass slide, trapping starts a distance l from the exit window, with the glass slide placed at d from the exit window, the energy in the dot should be decreased roughly by d/l. (In arriving at this, we assume that the light diffracted by the glass slide does not re-focus again.) On the other hand, if light is not trapped after the focus, the energy density of the dot appearing at the exit end would not be affected much by the glass slide. Experimental results showed that the latter was the case. We can further rule out re-focusing of

the diffracted light by focusing our camera system through the exit window of the cell at the glass slide inside the liquid. If the diffracted light re-focused, we should see a blurred spot; otherwide we should see a clear image of the dot from light diffracting at the glass slide. We did see a clear spot, and thus ruled out re-focusing. From these experiments, we can conclude that there is no substantial trapping after the focus.

Now we must see whether laser light was indeed converted to Raman light. If Raman light was generated along the focal spot motion path, we should expect to see longer Raman pulse duration for longer cell length, or for higher input power (since both increases the focal spot path length inside the cell) if we arrange to have the detector collect all Raman light generated in the cell. The experimental results confirmed the above prediction as shown in Fig. 25.

Next we showed that the Raman light generated is divergent rather than trapped. (Since trapping is independent of frequency, this answers the hypothetical question: if laser light were not converted into Raman light, would it be trapped?) We showed this by re-arranging our detection system so that only signal emerging from regions close to the exit window was admitted to the detector. For a trapped beam, this would not change anything since light only emerges from the exit window anyway. For the case where light diverges after the moving focus, we should see shortening of the pulse duration and decreasing of energy content. Experimentally, again the latter was the case. Finally, if Raman shifted light is diverging from the focal spot, focusing our camera system inside the cell should yield a dot at Raman frequency. Experiments also confirmed this.

Lastly, we would like to investigate whether there was any

divergent laser light inside the cell. The experimental arrangement, shown in Fig. 26, differed from the usual setup (see Fig. 13) by having the detector close to L_2 so that all signal not blocked by the disc will reach the detector. This means that signal diverging from sources located up to 15 cm inside the cell will be detected (Fig. 13). The pulses detected in this manner were shown in Fig. 27. When the input power was just at threshold, the relatively long duration pulse observed was the same as what was observed earlier with the detector collecting light emitted near the end of the cell. This is to be expected since all the divergent light came from region close to the exit window at this power level. For higher input power, in addition to the short pulse observed earlier, another pulse appeared less than 1 nsec later. Since the first pulse must come from light emitted when the focal spot hit the exit window, from the time delay we see that the second pulse must come from the region where the focal spot was moving backward and should correspond to the region which gives the clear laser dot in pictures taken by focusing the cell. The dip between the two peaks was a manifestation of the high conversion into forward Raman light for the forward going region, and also agreed with the fact that no dot can be seen when focusing at this region inside the cell.

From all these experiments, we can conclude that for the forward moving branch of the focal-spot motion curve, most of the laser power is converted into Raman light in the focal region. The Raman light is not trapped but leaks out all along the focal spot motion path. At the exit window, Raman conversion was limited since the window intercepts the focal spot, and then the dot at the laser frequency can be seen.

3. We now check the MFS model by comparing its predictions on frequency broadening of light from filaments with experimental results.

From the discussion in the theoretical section, we see that, if the focal spot velocity is much faster than light velocity, there should be little or no spectral broadening. For focal spot velocity of a few times that of light velocity, which corresponds to our experimental condition described in Part 1, our theory predicts a broadening of about 1 cm^{-1}. This broadening is observable since our laser spectral width is about .01 cm^{-1} (see Fig. 8).

To measure this, we used a Fabry-Perot interferometer with a plate separation of .5 cm (free spectral range of 1 cm^{-1}). The experimental setup is shown in Fig. 28, where as before, a disc was used to block off the background light. The experimental results in Fig. 28 shows that the broadening was about 0.3 cm^{-1}, we also see that the broadening increased as the input power increased. All these results are in good agreement with the prediction of the MFS model.

To see broadening of the order of 100 cm^{-1}, as observed commonly with multimode input laser, our theory requires a focal spot velocity of about 1.1 times the light velocity. To achieve this with an 8-nsec pulse, the cell length would have to be about 100 cm. On the other hand, this condition can be reached with a cell length of 35 cm if the duration of the input laser pulse is changed to about 1.5 nsec. Such a laser pulse can easily be obtained by weakly mode-locking a ruby laser.

To verify our prediction, we used a mode-locked ruby laser with a single transverse mode. The length of the cavity was 100 cm and the beam diameter was ~ 250 μ at the entrance window of the cell. Typical mode-locked trains are shown in Fig. 29, where each mode-locked

pulse has a full width at half-maximum of 1.6 nsec and the peak power of the highest pulse is about 120 kW. The spectral width of the laser output was always equal to the inverse of the pulse duration. Photographs taken at the end of the cell showed a single filament for each laser shot. However, the single filament on the photograph was in fact a superposition of several (often 2 or 3) filaments created consecutively by several pulses in the mode-locked train. This was seen from the oscilloscope trace of the filament pulses shown in Fig. 29a. That self-focusing or filament formation was terminated after a few pulses was probably due to thermal or acoustic effect resulting from stimulated light scattering in the liquid. In Fig. 29b, we recorded simultaneously the Raman pulses emitted from the filaments. The stimulated Brillouin scattering was not observed, presumably being suppressed because of the transient effect. Whenever the filament pulses were present, the laser pulses were clearly depleted, as shown in Fig. 29c. Comparison of the energy in the Raman pulses with the depleted energy in the laser pulses showed that the laser power was mainly depleted by stimulated Raman scattering.

In order to study the spectrum of light emitted from the filament, we used a Jarrell-Ash 1.5 meter Fastie spectrograph with its entrance slit widely open. The magnified (× 10) image of the filament at the end of the cell was recorded. A typical spectrum of the filament is shown in Fig. 30a. The appreciable spectral broadening and its semi-periodic structure are manifestations of significant phase modulation of light emitted from the filament.[31-33] The semi-periodic structure is somewhat smeared because the spectrum is actually a superposition of the spectra of several filaments as we mentioned earlier. A dot

with no spectral broadening is also visible at the laser frequency on the spectrum. It corresponded to the image of the ~ 10 μ filament, and apparently came from the non-trapped part of the self-focused beam. The Stokes Raman spectrum from the filament is also shown in Fig. 30a. It has the same characteristics as the spectrum around the laser frequency and shows that the Raman radiation from the filament is even more strongly phase-modulated.

From our theoretical analysis,[21] we expected to find in our case a broadened spectrum of the order of 100 cm^{-1} if the peak power of a mode-locked pulse was above 100 kW. For lower peak power, the broadening would be less, and for peak power less than 60 kW, we expected to see no appreciable spectral broadening at both laser and Raman frequencies. This was roughly what we observed. At high peak power, the superposition of the spectra of several filaments and the effects of the filaments on one another made quantitative analysis difficult. Denariez-Roberge and Taran[18] showed spectral broadening increased with the filament length. This can also be shown to be in qualitative agreement with our model.

To see whether light is trapped by the moving focus, we focused the image of the beam cross-section at several cm inside the cell on the spectrograph. No extended spectral broadening was ever seen at either the laser or the Raman frequency. The fact that only light emitted from filaments at the end of the cell showed spectral broadening gave clear evidence that it was the trapped part of the light which gave rise to the broadened spectrum. Occasionally, we observed clear images of the focal spot at both laser and Raman frequencies, as shown in Fig. 30b. They corresponded to the case where the peak power of the input pulse was low, so that the self-focused light was not

being trapped over any appreciable distance, with the result of little spectral broadening.

Although the results presented here are all on toluene, we have performed similar experiments on CS_2. There was no qualitative difference between the two cases, except that spectral broadening in CS_2 was several times more appreciable. We therefore conclude, from our experimental results, that the observed small-scale filaments are actually composed of moving focal spots, but under suitable conditions, the self-focused light can be partially trapped in the dielectric channels established temporarily by the moving focal spots. The condition for trapping can be easily fulfilled with the use of a mode-locked laser or a multimode Q-switched laser.

IV. DISCUSSION AND CONCLUSIONS

We have seen in Section III how the MFS model successfully explained our experimental observations using lasers with controlled output beams. We now examine other experiments and their interpretations reported in the literature in light of this model. We will also discuss effects that are not explained by the MFS model.

A. Experiments with Laser Beams that are "Spatially Smooth"

We note that the spatial distribution criterion required here is somewhat different from what is usually called a "single transverse mode" beam. What is required here is any smooth spatial distribution with an intensity maximum at the center and decreases monotonely with radial distance. On the other hand, in many cases, the output of a pulsed laser may consist of, say, 95% of TEM_{oo} mode admixed with 5% higher order modes. This beam will appear to be "diffraction limited" for all practical purposes;and, in fact, for many experiments, such a beam can be taken as TEM_{oo} mode in the data analysis, without noticeable error. This, however, is definitely not the case in studying self-focusing and filaments. As shown by Bespalov and Talanov,[16] an intense beam with power density F in a nonlinear medium is unstable against spatial perturbation with characteristic size

$$\Lambda = \lambda_o \, C^{1/2}/(16\pi n_o^2 \, n_2 F)^{1/2}$$

where F = power/unit areas. For F = 50 MW/cm^2, $n_2 \sim 10^{-11}$ esu (CS_2) $\Lambda \sim 100\ \mu$.

Small intensity inhomogeneities of this size will thus start self-focusing independent of the rest of the beam. This explains why, in many cases, laser beams that are apparently diffraction limited

single transverse mode can produce multiple filaments.[10] (Direct experimental evidence of this was obtained by Abbi and Mahr.[36])

Thus, by "spatially smooth" laser beam, we mean that the laser beam will consistently self-focus to a single filament. We stress that only in this case we can claim any knowledge of the initial conditions for the filament formation.

A number of experiments with this kind of input condition have been reported in the literature,[20,28,29,35] in addition to ours described in Section III. The properties of filaments reported there agreed very well with our observations. The few seemingly different observations can be traced back to the difference in the input conditions such as the initial beam size, the input pulse duration and cell lengths, etc.

For example, in the experiment of Korobkin, et al.,[20] in which the motion of the focal spot was measured using a fast streak camera, backward motion was observed. This is due to their longer input pulse duration (15 nsec) and short cell length (10 cm), under which the focal spot is in the backward moving region.

Similarly, Maier et al.[28] performed an experiment studying the backward Raman-filament correlation similar to ours and they concluded that the Raman signal originated close to the exit window of the cell independent of input power, quite different from what we observed in Section III. This is due to their longer input pulse duration (30 nsec compared to our 8 nsec) and larger beam size (~ 600 μ compared to our 300 μ). Under these conditions, the first focal spot would appear at the end of the cell, moving inward at a velocity close to or smaller than light velocity in the medium, for a wide range of input peak power. This explains why the Raman pulse always originated from close

to the exit end of the cell.

The experimental results of Maier, et al.[29] on the interaction between self-focusing and stimulated scattering agreed well with our observation. Their analysis and interpretation can be further clarified using the MFS model. Under their experimental conditions (25 nsec pulse duration, 435 μ beam diameter and 30 cm cell length) the first focal spot should appear at the end of the cell. Backward Raman and Brillouin is initiated by this focal spot and quickly depletes the incoming light. Due to this depletion, the subsequent transmitted laser power would be lower than this power level which initiates the backward stimulated processes. Therefore, the peak value of the transmitted power in this case is equal to the power level with which the beam focuses at the end of the cell, and is the value one should use to calculate the diameter of the focused beam at the end of the cell. This value of input power was used in the analysis of Ref. 29, through somewhat different reasoning. We note that in general the peak transmitted power corresponds to the level at which backward stimulated Raman scattering is initiated and might not be related to the power level which determines the diameter of the focus beam at the exit end.

B. Experiments with Spatially Inhomogeneous Laser Beam

Under this type of input condition, tens and hundreds of filaments were observed,[10-12,32,18] due to breaking up of the beam.[16] We know very little about the input conditions for each filament, and quantitative comparison of experiments with theory is not possible. We can, however, make some qualitative comparison with the predictions of the MFS model.

We note that, for an inhomogeneous beam, even though the total power integrated over the entire beam might have a "smooth" time

variation of the order of 10 nsec, the time variations of the "hot spots" which give the filaments are commonly in the range of 1 nsec or shorter.[36] Under these conditions, each filament is likely to be formed through self-focusing of the beam from a hot spot of ~ 50 μ in diameter, with a pulse duration of ~ 1 nsec and a power level of the order of P_{cr}.[16,23]

With this kind of input conditions in mind, the experimental results of Denariez-Roberge, and Taran[18] can be easily explained using the MFS model. In view of the probably small initial diameters (~ 100 μ) of the hot spots, it is not surprising that filaments were still present after the laser beam passed through a screen with 30 μ holes. They also showed that, in their experiment, the number of filament dots at the exit window decreased (statistically) by a factor of 3 when a 1mm thick glass flat was inserted inside the liquid. We expect this to happen in the MFS model since the glass slide will disrupt by diffraction the focusing action of a small-size beam containing a power not much larger than P_{cr}. (We note that in our experiments at $P \simeq 2 P_{cr}$, the single filament dot appeared at the exit window even when a glass slide of 3mm was inserted inside the liquid (see Section III). Finally, for the dependence of spectral broadening of light from the filaments on their propagation distance, we showed in Section II that their results can be explained by the MFS model.

C. Experiments Using Picosecond Input Pulses

Filaments have been observed under picosecond excitation,[19] with properties quite similar to those observed under multimode nanosecond excitation. In all of the experiments,[19,37,38] more than one filament were observed per shot. This is apparently due to the extremely high

power densities in these beams (~ 5 GW/cm^2), so that the beam in the nonlinear medium will break up with the slightest intensity fluctuations or perturbations.

One of the chief reasons for studying filaments under picosecond excitation is to try to determine the physical mechanisms responsible for the intensity dependent nonlinear refractive index.[19] It was suggested[38] that information could be obtained by analyzing the spectral broadening of light from the filament, assuming that the short filament pulse propagates in the self-trapping mode.[33] (For example, the ratio between the extents of the spectral broadening on the Stokes and anti-Stokes sides was used to set a limit on the value of the relaxation time τ of the nonlinear refractive index.[38]) We have seen that, under nanosecond input conditions, filaments are the tracks of moving focal spots rather than self-trapped waveguides. Now, can the moving focal spot model also explain the observed filament properties under picosecond pulse excitation?

First, we note that, while self-trapping solutions of Eq. (5) have been obtained in the limit $\tau \to 0$, it is not clear whether self-trapping solution exists for a pulse with duration comparable to τ, when τ is finite. In fact, since the medium cannot respond instantaneously to give a Δn large enough for self-trapping, the field intensity in the leading edge of the pulse will decrease continuously through diffracting as the pulse propagates along. (This effect can be seen in the solution of Fleck and Kelly[24] that a symmetric pulse develops into an asymmetric pulse through self-focusing.) Thus, in a medium where $\tau \neq 0$, self-trapping with constant pulse shape (as assumed in Gustafson, et al.[33] and Cubeddu et al.[38]) seems to be impossible. Secondly, it has been pointed out[39,41] that since the positions of the maxima and

minima in the broadened filament spectrum appeared to be independent of the radial distance r of the filament, one can conclude that the phase modulation in time must be independent of r. According to the self-trapping model, the phase change $\Delta\phi(r)$ is given by $k\Delta n(r)\ell$ where ℓ is the length of the filament (Eq. (15a)) and thus Δn must be independent of r. On the other hand, the intensity distribution $|E|^2(r)$ of the filament has been shown to be roughly Gaussian.[19,39] In order to have Δn independent of r induced by a Gaussian intensity distribution, Δn must be completely saturated with respect to $|E|^2$ over nearly the entire intensity distribution. This appears to be unlikely in view of the relatively low values of Δn and $|E|^2$ observed in experiments.[37-39] (The lack of spatial dependence of $\Delta\phi$ was also verified in Ref. 39 by measuring the spatial Fourier transform of light from the filament.)

Let us now consider the MFS model under picosecond excitation. Although our discussion on this model so far has been limited to input pulses with duration much longer than the relaxation time τ, the qualitative aspects of the theory should hold even for the case of ultrashort pulses. We realize that, if the input pulsewidth is comparable with τ, then the transient response of the medium should affect the self-focusing distance. For the upper branch of the U-curve in Fig. 1, the beam with an input power P should now self-focus at a distance larger than the value given by Eq. (11), but the curve should still retain its qualitative feature. Also, because of transience, the dimension of the focal spot would be larger. The transient effect on the lower branch of the U curve may be even more drastic, since self-focusing of the lagging part of the input pulse may now be affected by self-focusing of the leading part. From our

theory, we can make the following qualitative predictions for the case of ultrashort pulses. The duration of the output filament pulse should still be of the order of τ. Spectral broadening with semi-periodic structure should be greatly enhanced, with Stokes and anti-Stokes broadening equally pronounced. In this case, light may also be partially trapped in the track of the moving focal spot over a much longer distance. These predictions explain qualitatively the recent experimental results obtained with picosecond mode-locked pulses.[37,38]

We note that the MFS model does not have the inconsistencies mentioned earlier with the STF model. In particular, the fact that the position of the maxima and minima in the broadened spectrum is independent of r appears to be consistent with the MFS model. In fact, to give such a spectrum, all we need, for example, is a refractive index change of the form $\Delta n = \Delta n_1(r)\,\Delta n_2(z,t)$ together with an intensity distribution of the form $|E|^2 = A_1(r)\,A_2(z-c't)$ where $\frac{\partial}{\partial r}\Delta n_1(r) \approx 0$ for the range where $A_1(r)$ is non-zero. (The functional form for Δn in Ref. 38 is incorrect. This is due to their assumption that $\Delta\phi = S_1(z,t) + S_2(r_1 z)$ inside the filament. In their subsequent calculation, however, they use that form of $\Delta\phi$ for all space, which lead to their erroneous conclusion.) These forms of Δn and $|E|^2$ are certainly allowed in the MFS model. Whether such distributions can indeed exist in the track of a moving focus can only be determined by detailed solution of the focal region under picosecond excitation.

D. Some Unexplained Effects

1. Limiting Size of the Filament

We realize that the diameter of the filament should correspond to the diameter of the focal spot. However, no numerical calculation

has yet been able to go beyond the focal region and to predict the focal spot dimensions. Transient effects are important close to the focus since the high-intensity focal spot is moving at a very high speed. Various stimulated scattering in the focal region may also come into play through depletion of the laser power and generation of heat in the focal region. Above all, the dielectric response $\Delta n(|E|^2)$ of the medium to the field plays a central role in deciding how the beam is self-focused.

Recently, self-focusing of light due to the intensity-dependent dispersion of a resonance line[42] has been observed by Grischkowsky.[43] In this system, Δn as a function of $|E|^2$ is known accurately and no stimulated scattering is present due to the low power needed for self-focusing. Thus calculation[44] can be carried out through and beyond the focal region to compare with experimental results. Information obtained in this system concerning the limiting size of the filament should be useful in determining the physical mechanisms involved in the liquid case.

2. Side View of the Filament

The physical mechanisms behind the strong scattered light emitted by the filament normal to its propagation direction[11,40] remains unknown. The origin of the beating pattern along the filament observed by Brewer and Townes,[40] and the high value of Δn deduced, cannot be explained .

E. Summary and Conclusion

We have presented a systematic study of small-scale filaments. We described the two theoretical models (MFS model and STF model) and compared their predictions with existing data in the literature. We also presented a calculation based on the MFS model to obtain the

spectral broadening of light from filaments. Experimentally, extensive measurements on filaments were performed under known input conditions. The relations between the input condition, the stimulated scattering processes present, and the filament properties were studied. Based on these observations, specific experiments were designed and carried out to distinguish the two models experimentally.

Results obtained from these experiments agreed quantitatively with the predictions from the MFS model. We also show that experimental results on filaments reported in the literatures can be explained satisfactorily by the MFS model.

We therefore conclude that small-scale filaments are formed as the result of moving focal spots. This is definitely true for nanosecond pulse excitation and is also likely to be true for picosecond pulse excitation.

ACKNOWLEDGEMENTS

I am deeply grateful to my thesis advisor, Professor Y. R. Shen, for his invaluable guidance throughout the course of this work, for his patience during the many hours of discussion, and for his encouragement when things did not look bright.

I would like to thank Professors C. H. Townes, R. Y. Chiao, T. K. Gustafson, and Dr. P. L. Kelley for fruitful discussions during various phases of my work. I also thank the many members in Professor Shen's group, from whom I learned much through daily discussions. Among them, I especially thank Dr. Dillard Faries, from whom I learned many techniques needed during my first year of research.

I would like to thank Kathy Williams for preparing the manuscript and for her sincere effort to make our lives as graduate students easier and more pleasant.

I thank my parents who made it possible for me to receive my education and gave me much encouragement and advice throughout the course of it.

I thank my wife, Ivy, for her continual support, encouragement, and understanding throughout this work.

I gratefully acknowledge the financial support given to me during the last two years as an IBM Fellow.

This work was performed under the auspices of the U. S. Atomic Energy Commission.

REFERENCES

1. G. A. Askarjan, Zh. Eksperim. i Teor. Fiz. 42, 1567 (1962). [English transl.: Soviet Phys.--JETP 15, 1088 (1962)].
2. V. I. Talanov, Izv. Vysshikh Vchebn. Zavedenii, Radiofiz. 7, 564 (1964). [English transl.: Radiophysics 7, 254 (1964)].
3. R. Y. Chiao, E. Garmire, and C. H. Townes, Phys. Rev. Letters 13, 479 (1964).
4. P. L. Kelley, Phys. Rev. Letters 15, 1005 (1965).
5. V. I. Talanov, Zh. Ekspirim. i Teor. Fiz. Pis'ma v Redaktsiyu 2, 218 (1965). [English transl.: Soviet Phys.--JETP Letters 2, 138 (1965)].
6. S. K. Akhmanov, A. P. Sukhorukov, and R. V. Khokhlov, Zh. Ekspirim. i Teor. Fiz 50, 1537 (1966). [English transl.: Soviet Phys.--JETP 23, 1025 (1966)].
7. N. E. Pilipetskii and A. R. Rustamov, ZhETF Pis. Red. 2, 88 (1965). [JETP Lett. 2, 55 (1965)] G. Hauchecorne and G. Mayer, Compt. Rend. 261, 4014 (1965).
8. Y. R. Shen and Y. J. Shaham, Phys. Rev. Letters 15, 1008 (1965). P. Lallemand and N. Bloembergen, Phys. Rev. Letters 15, 1010 (1965). C. C. Wang, Phys. Rev. Letters 16, 344 (1966).
9. E. Garmire, R. Y. Chiao, and C. H. Townes, Phys. Rev. Letters 16, 347 (1966).
10. R. Y. Chiao, M. A. Johnson, S. Krinsky, H. A. Smith, C. H. Townes, and E. Garmire, IEEE J. Quantum Electron. QE-2, 467 (1966).
11. R. G. Brewer and J. R. Lifsitz, Phys. Letters 23, 79 (1966).
12. R. G. Brewer, J. R. Lifsitz, E. Garmire, R. Y. Chiao, and C. H. Townes, Phys. Rev. 166, 326 (1968).

13. T. K. Gustafson, P. L. Kelley, R. Y. Chiao, and R. G. Brewer, Appl. Phys. Lett. 12, 165 (1968).

14. W. G. Wagner, H. A. Haus, and J. H. Marburger, Phys. Rev. 175, 256 (1968).

15. E. L. Dawes and J. H. Marburger, Phys. Rev. 179, 862 (1969).
V. N. Goldberg, V. I. Talanov, and R. E. Erm, Izv. Vysshikh Vchebn. Zavedenii Radiofiz. 10, 674 (1967).

16. V. I. Bespalov and V. I. Talanov, ZhETF Pis. Red. 3, 471 (1966). [English Transl.: Soviet Phys. - JETP Letters 3,307 (1966).]

17. V. N. Lugovoi and A. M. Prokhorov, ZhETF Pis. Red., 7, 153 (1968). [English Transl.: Soviet Phys. - JETP Lett. 7, 117 (1968).]
A. L. Dyohko, V. N. Lugovoi, and A. M. Prokhorov, ibid. 6, 655 (1967). [JETP Lett. 6, 146 (1967).]

18. M. M. Denariez-Roberge and J.-P. E. Taran, Appl. Phys. Lett. 14, 205 (1969).

19. R. G. Brewer and C. H. Lee, Phys. Rev. Lett. 21, 267 (1968).
R. Polloni, C. A. Sacchi, and O. Svelto, Phys. Rev. Lett. 23, 690 (1969).
R. R. Alfano and S. L. Shapiro, Phys. Rev. Lett. 24, 584, 1217 (1970).

20. M. M. T. Loy and Y. R. Shen, Phys. Rev. Lett. 22, 994 (1969).
G. M. Zverev, E. K. Maldutis, and V. A. Pashkov, ZhETF Pis. Red. 9, 108 (1969). [English Transl.: JETP Lett. 9, 61 (1969).]
V. V. Korobkin, A. M. Prokhorov, R. V. Serov, and M. Ya. Shchelev, ZhETF Pis. Red. 11, 153 (1970). [English Transl. JETP Letters 11, 94 (1970).]
M. M. T. Loy and Y. R. Shen, Phys. Rev. Lett. 25, 1333 (1970).

21. Y. R. Shen and M. M. T. Loy, Phys. Rev. A, June 1971 (to be published). (presented at the 6th Inter. Quantum Electronics Conf. at Kyoto, Japan Sept. 1970).

22. J. Frenkel, Kinetic Theory of Liquids (Dover, N.Y., 1945).

23. C. S. Wang, Phys. Rev. 173, 908 (1968).

24. J. A. Fleck, Jr. and P. L. Kelley, Appl. Phys. Lett. 15, 313 (1969).

25. For example, Y. R. Shen, M. Y. Au Yang, and Marvin Cohen, Phys. Rev. Lett. 19, 1171 (1967).

26. M. M. T. Loy and Y. R. Shen, Phys. Rev. Letters 22, 994 (1969); 25, 1333 (1970).

27. A. A. Abramov, V. N. Lugovoi, and A. M. Prokhorov. ZhETF Pis. Red. 9, 675 (1969). [English Transl. JETP Lett. 9, 419 (1969).]
T. K. Gustafson and J.-P. E. Taran, IEEE J. Quantum Electronics QE-5, 381 (1970).

28. M. Maier, W. Kaiser, and J. A. Giordmaine, Phys. Rev. Lett. 17, 1275 (1966), and Phys. Rev. 177, 580 (1969).

29. M. Maier, G. Wendl, and W. Kaiser, Phys. Rev. Lett. 24, 352 (1970).

30. F. Shimizu and B. P. Stoicheff, IEEE J. Quantum Elec. QE-5, 544 (1969). A much higher value of $\Delta n=0.2$ was deduced by R. G. Brewer and C. H. Townes, Phys. Rev. Lett. 18, 196 (1967).

31. F. Shimizu, Phys. Rev. Lett. 19, 1097 (1967), R. G. Brewer, Phys. Rev. Lett. 19, 8 (1967).

32. A. C. Cheung, D. M. Rank, R. Y. Chiao, and C. H. Townes, Phys. Rev. Lett. 20, 786 (1968).

33. T. K. Gustafson, J.-P. E. Taran, H. A. Hans, J. R. Lifstiz, and P. L. Kelley, Phys. Rev. 177, 306 (1969).

34. J. R. Lifsitz and H. P. H. Grieneisen, Appl. Phys. Lett. 13, 245 (1968).

35. V. V. Korobkin and R. V. Serov, ZhETP Pis. Red. 6, 642 (1967). [English Transl. JETP Lett. 6, 135 (1967).]

36. S. C. Abbi and H. Mahr, Phys. Rev. Lett. 26, 604 (1971).

37. R. L. Carmen, J. Reinjes, and F. Shimizu (private communication).

38. R. Polloni, C. A. Sacchi, and O. Svelto, Phys. Rev. Letters 23, 690 (1969).

39. R. Cubeddu, R. Polloni, C. A. Sacchi, O. Svelto, and F. Zavaga, Phys. Rev. Lett. 26, 1009 (1971).

40. R. G. Brewer and C. H. Townes, Phys. Rev. Lett. 18, 196 (1967).

41. R. Y. Chiao (private communication).

42. A. Javan and P. L. Kelley, IEEE J. Quantum Electron., QE-2, 470 (1966).

43. D. Grischkowsky, Phys. Rev. Lett. 24, 866 (1970).

44. J. A. Armstrong (private communication).

45. The values of input power, beam diameter, and cell lengths in our experiments were such that only one focal spot would exist, according to Fig. 2 of Abramov, et al. (reference 27). Unless otherwise stated, we will assume that this is the case in our theoretical discussion.

FIGURE CAPTIONS

Fig. 1. The lower trace describes the input power P(t) as a function of time t. The peak power is 42.5 Kwatts and the half width at the e^{-1} point is 1 nsec. The upper trace, calculated from Eq. (1), describes the position of the focal spot as a function of time. The values of P_{cr} and K used are 8 Kwatts and 11.6 cm-$(KW)^{1/2}$ respectively, which correspond roughly to an input beam of 400μ in diameter propagating in CS_2. The dotted lines, with the slope equal to the light velocity in CS_2, indicate how the light propagates along the z-axis at various times.

Fig. 2. Velocity of the focal spot for the case described in Fig. 1.
(a) as a function of time t, and
(b) as a function of distance z.

Fig. 3. Paths of the laser light (with slope c/n_o) and the backward stimulated radiation (with slope c/n_o) generated by the focal spots at A and B.

Fig. 4. Spectral broadening in CS_2 (Reproduced from Gustafson et al.[33])
(a) Theoretical calculation of Cheung et al.[32]
(b) Experimental spectrum of Cheung et al.[32]
(c) Theoretical calculation of Gustafson et al.[33] assuming an initially Gaussian intensity profile. The full(1/e) width equals 7.4 psec.

Fig. 5. (a) Normalized power P_f of the filament pulse vs time; ($P_{f\,max}$ = 11.2 KW);
(b) Field-induced phase change $\Delta\phi$; ($\Delta\phi_{max}$ = 129.3 rad.);
(c) Power spectrum of the filament pulse obtained from the Fourier transform of $P_f^{1/2} \exp(i\Delta\phi)$.

The velocity of the focal spot at $z = \ell$ is 1.124 c'.

Fig. 6. Curves describing P_f vs t, $\Delta\phi$ vs t, and the power spectrum of the filament pulse obtained with all parameters in Fig. 5 kept unchanged except $\tau' = 6 \times 10^{-12}$ sec.

Fig. 7. Curves describing P_f vs t, $\Delta\phi$ vs t, and the power spectrum of the filament pulse obtained with all parameters in Fig. 5 kept unchanged except $\tau' = 10^{-11}$ sec.

Fig. 8. Curves describing P_f vs t, $\Delta\phi$ vs t, and the power spectrum of the filament pulse obtained with all parameters in Fig. 5 kept unchanged except that the decay of $P_f(t)$ is linear and symmetric to the linear rise of P_f.

Fig. 9. Typical input laser pulse (time scale: 10 nsec/div) and its Fabry-Perot pattern (free spectral range: .4 cm^{-1}).

Fig. 10. Experimental set up (a) and pictures of the beam cross sections (at constant cell length ℓ = 16cm) at increasing input power levels from (a) to (d). At higher powers, the observed beam (filament) size is independent of power level. A collection of filaments with this limiting size (about 5μ) are shown in (e). The liquid used was CS_2.

Fig. 11. Densitometer trace of a CS_2 filament.

Fig. 12. Filament size in CS_2-nitrobenzene mixture. Approximately five shots were taken at each concentration. Sizes were determined from densitometer traces like Fig. 11.

Fig. 13. (a) Experimental setup to measure the direction of the filament, blocking the unfocussed background light from entering the detector. (L_1, L_2, converging lenses; plane E, end of liquid cell; plane A, image plane of E; plane B, detector.)

(b) Schematic drawing to show the discrimination against light diverging from deep inside the cell.

(c) Percentage of light signal from source at a distance d from the end of the cell that will reach the detector. Light intensity is assumed to be constant within the core angle of 4×10^{-2} radian and zero outside.

Fig. 14. Filament pulse durations in toluene, at constant cell length (32.5cm), when input power was increased from (a) to (d).

Fig. 15. (From Loy and Shen, Appl. Phys. Lett. 14, 380). Oscilloscope traces of the system response to various light pulses. The system was composed of an ITT F4018 photodiode in connection with a Tektronix 519 oscilloscope. (a) A mode-locked pulse of 8 ± 3 psec in pulse width from a Nd-glass laser. (b) A "filament" pulse with a pulse width of 190 ± 30 psec and an asymmetric pulse sahpe as shown in the insert. (c) A "filament" pulse with a pulse width of 100 ± 60 psec. The inaccuracy is due to uncertainty in the pulse shape. The insert shows that the pulse width could be very different depending on whether the pulse is Gaussian or Lorentzian. The circles indicate results of computer calculation, taking the mode-locked pulse as a δ function.

Fig. 16. Focal spot motion curves for two input peak power values, $P_2 > P_1$. The two dotted lines represent the boundaries of the region monitored by the detection system.

Fig. 17. Experimental setup and data where the input power (P), the backward Raman radiation (BR), backward Brillouin radiation (B), forward Raman radiation (FR), filament pulse(F), and filament picutre (F_p) were simultaneously measured. (The filament picutres were too faint to be reproduced here.) The liquid used was toluene, and the cell length was 32.5 cm.

See text for more detail.

Fig. 18. Incident (P_i) and transmitted power (P_T) through a 26 cm toluene cell.

(a) Below threshold, no depletion of laser power.

(b) Above threshold, depletion occurred due to backward stimulated radiations.

Fig. 19. (a) Schematic diagram showing the relative positions of the backward Raman pulse and the filament pulse, as a function of time. The pulse separation at t_2 (when the focal spot is at the end of the cell) is defined as d.

(b) Schematic diagram showing that d should increase as the input peak power increases.

Fig. 20. The pulse separation d, measured at four different cell length was plotted as a function of input peak power. The solid curves are theoretical predictions using experimentally determined values of P_{cr} and K (Fig. 21).

Fig. 21. The inverse of the minimum self-focusing distance Z_f as a function of the square root of the input peak power P. The slope of this line gives the parameter K; and the intercept, the square root of P_{cr}.

Fig. 22. Schematic diagram to show that by measuring the value of d at different cell lengths, the velocity of the focal spot can be shown to be higher than light velocity c'.

Fig. 23. Time-of-flight experiment on the focal spot. The experimental set up, together with a typical oscilloscope trace is shown on the left. The solid curve on the right was obtained using experimentally determined parameters K, P_{cr}, and P(t). The dots with the error bars at 21 and 29.5 cm are results

obtained from direct measurements with respect to the focal spot appearing at the end of the cell (cell length 36 cm). The dashed line with a slope equal to the light velocity is shown for comparison.

Fig. 24. (a) Schematic drawing showing the optical setup where the plane S (inside the cell) is imaged through the lens L onto the plane F where the film is placed. Filament light emerging from the end of the cell (plane E) is shown as dotted lines which form a blurred image at F.

(b) Picture taken with optical system focusing at a plane 1.5 cm inside the cell. The medium was toluene, and the cell length 33.5. Magnification was about 100×.

Fig. 25. Forward Raman pulses with their input laser pulses at two cell lengths. For the same cell length (a and b, both at 42 cm), higher input power gave a Raman pulse with longer duration (b). For about the same input power (a and c), longer cell length gave longer Raman pulse (c).

Fig. 26. Experimental setup detecting signal up to 15 cm inside the cell (see Fig. 13c).

Fig. 27. Experimental data taken with setup shown in Fig. 26 to detect diverging laser light inside the cell.

(a) Input power at threshold for self-focusing.

(b) Input power above threshold.

Fig. 28. Experimental observation of the spectrum of the filament when the focal spot velocity was a few times light velocity. The input power, together with the Fabry-Perot pattern, showed that the broadening increased as the input power increased.

Fig. 29. (a) Interleafed input laser pulse train and filament pulses.

The laser pulses were optically delayed by 6 nsec with respect to the filament pulses. Three filament pulses appeared in this shot.

(b) Interleafed input laser pulse train (optically delayed by 6 nsec) and Raman Stokes pulses from the filaments recorded simultaneously with (a).

(c) Interleafed input and transmitted laser pulse trains showing depletion of laser energy. The input pulses were optically delayed by 6 nsec with respect to the transmitted pulses. They correspond to the train with lower amplitude.

Fig. 30. Laser and Raman Stokes spectra of a filament created by self-focusing of 1.6 nsec mode-locked pulses in a 37 cm toluene cell, (a) taken with the spectrograph focused at the end of the cell; (b) taken with the spectrograph focused inside the cell (at 1.5 cm from the end of the cell). The laser spectra are on the left with the slit images centered at 14402 cm^{-1} and the Stokes spectra on the right with the slit images centered at 13400 cm^{-1}.

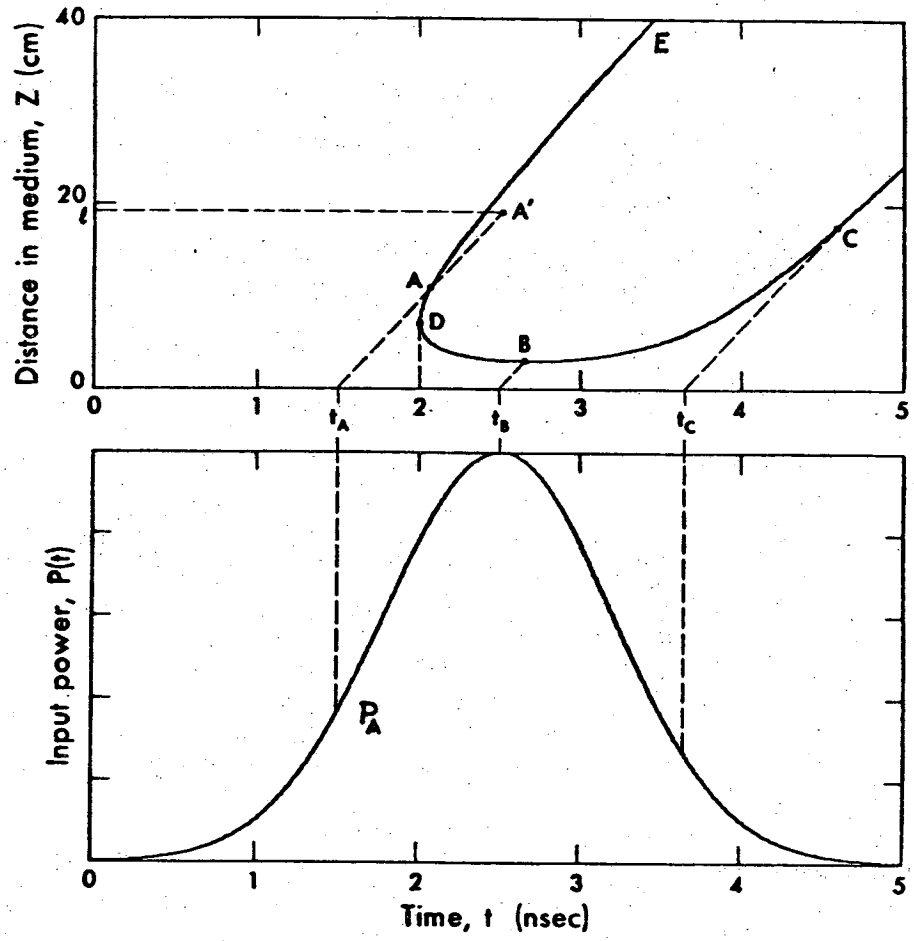

XBL7010-6788A

Fig. 1

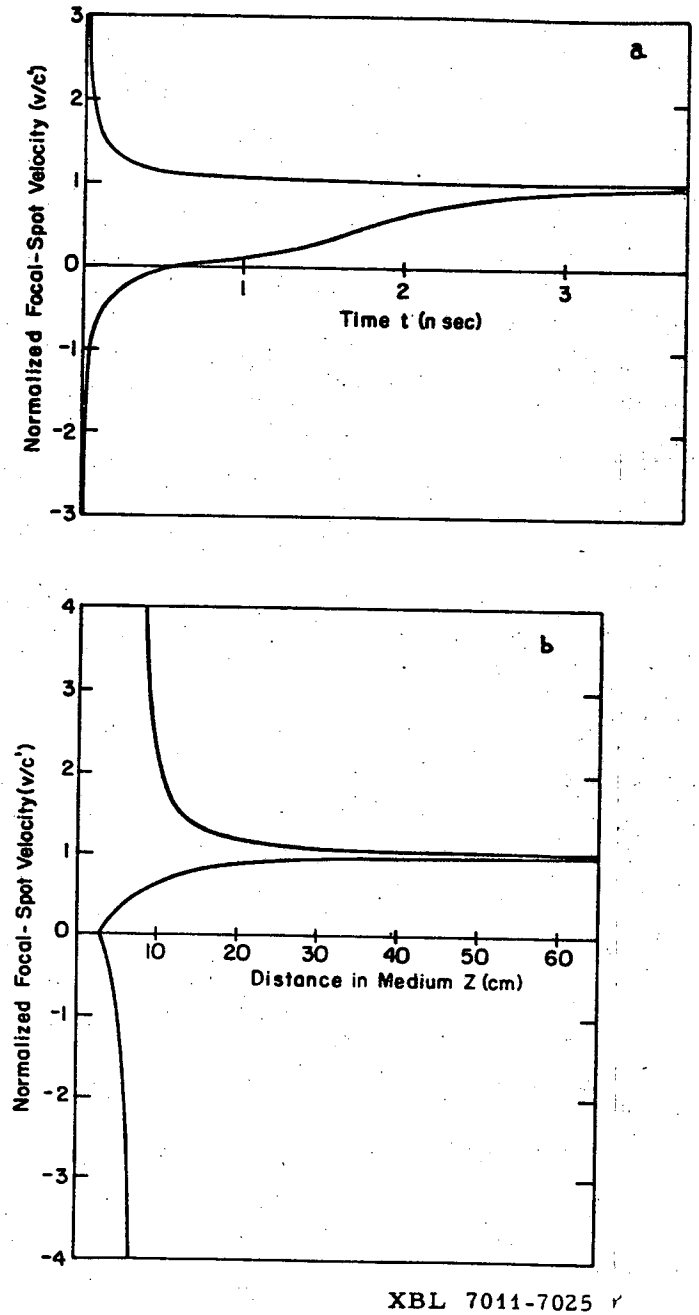
a
Normalized Focal-Spot Velocity (v/c)
Time t (n sec)
b
Normalized Focal-Spot Velocity(v/c')
Distance in Medium Z (cm)
XBL 7011-7025

Fig. 2

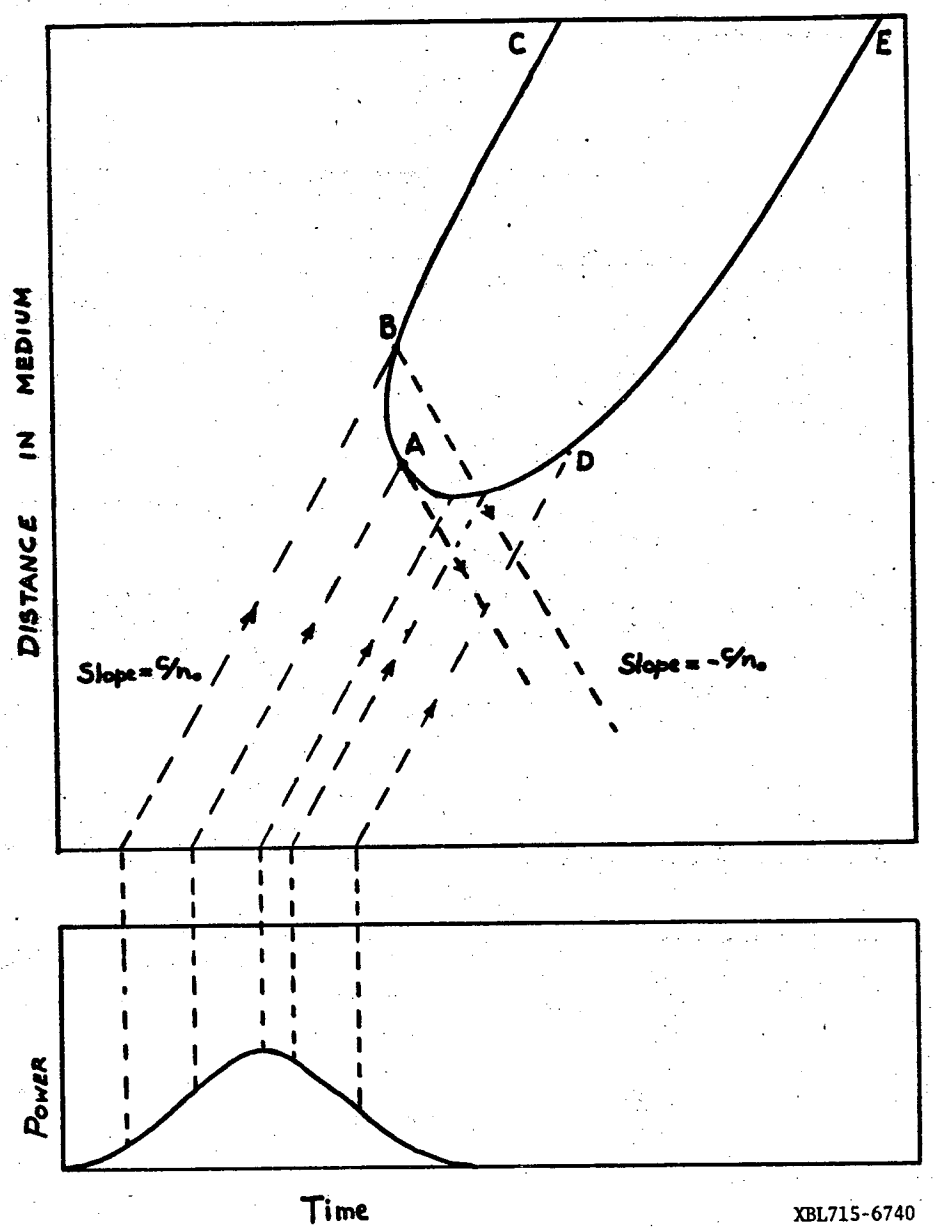
C
E
B
A
D
DISTANCE IN MEDIUM
Slope = c/n₀
Slope = -c/n₀
POWER
Time
XBL715-6740

Fig. 3

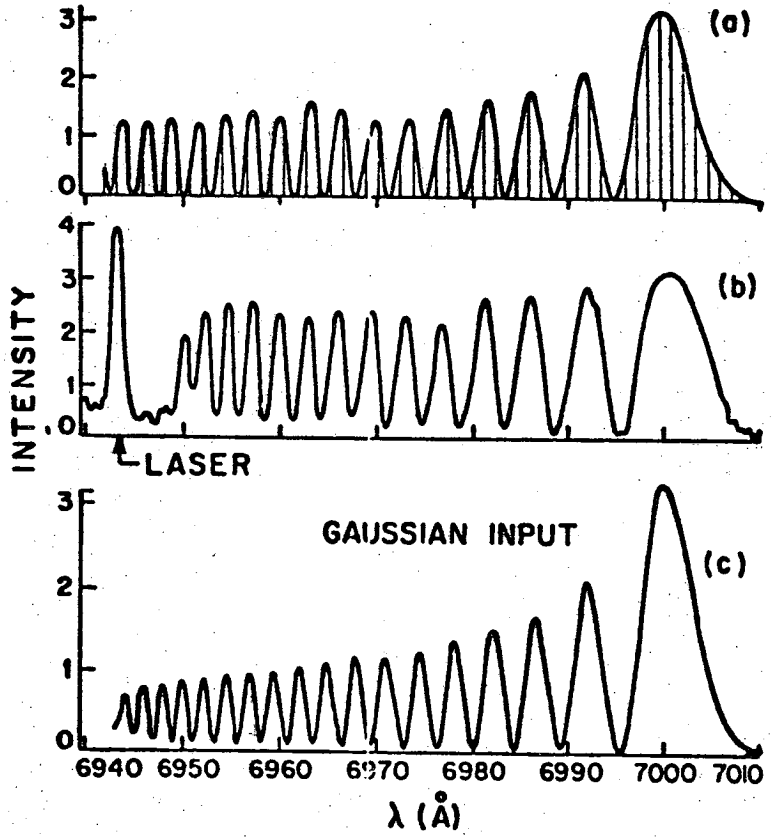

Fig. 4

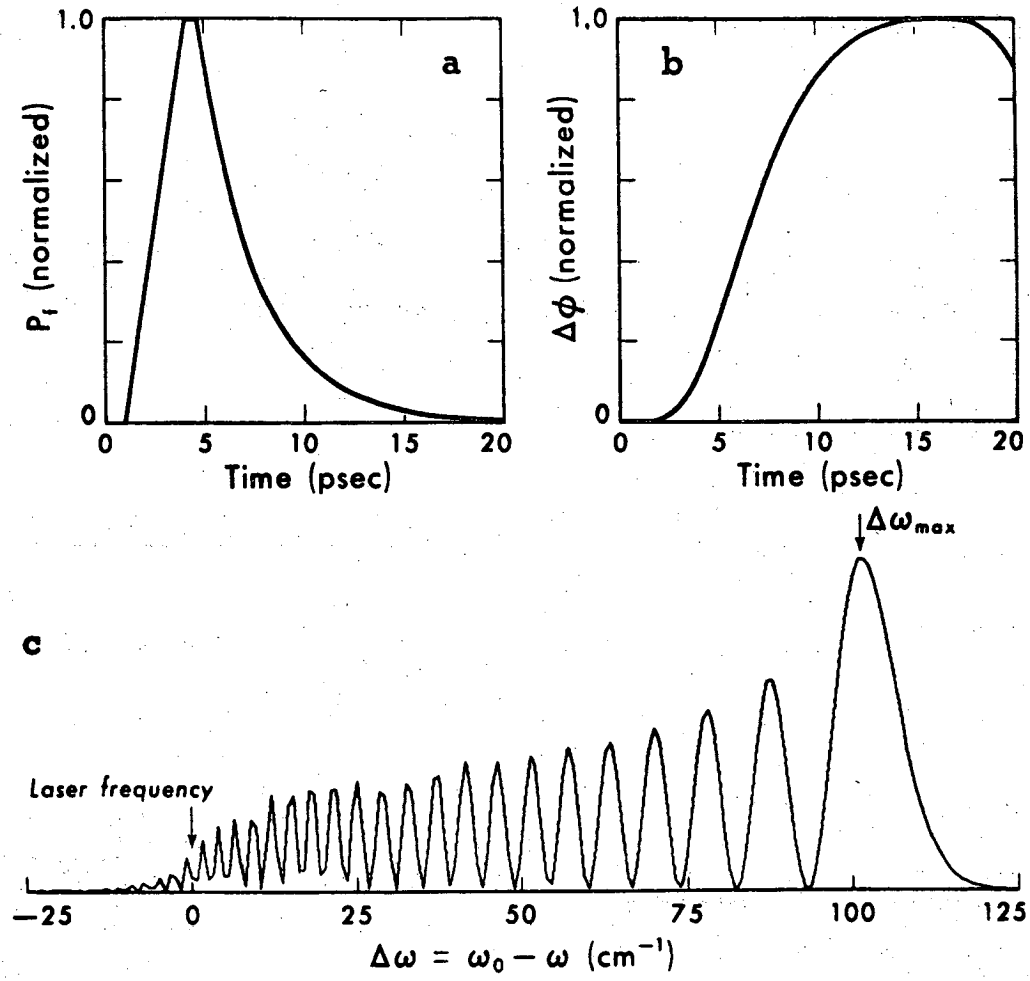

XBL 711-31

Fig. 5

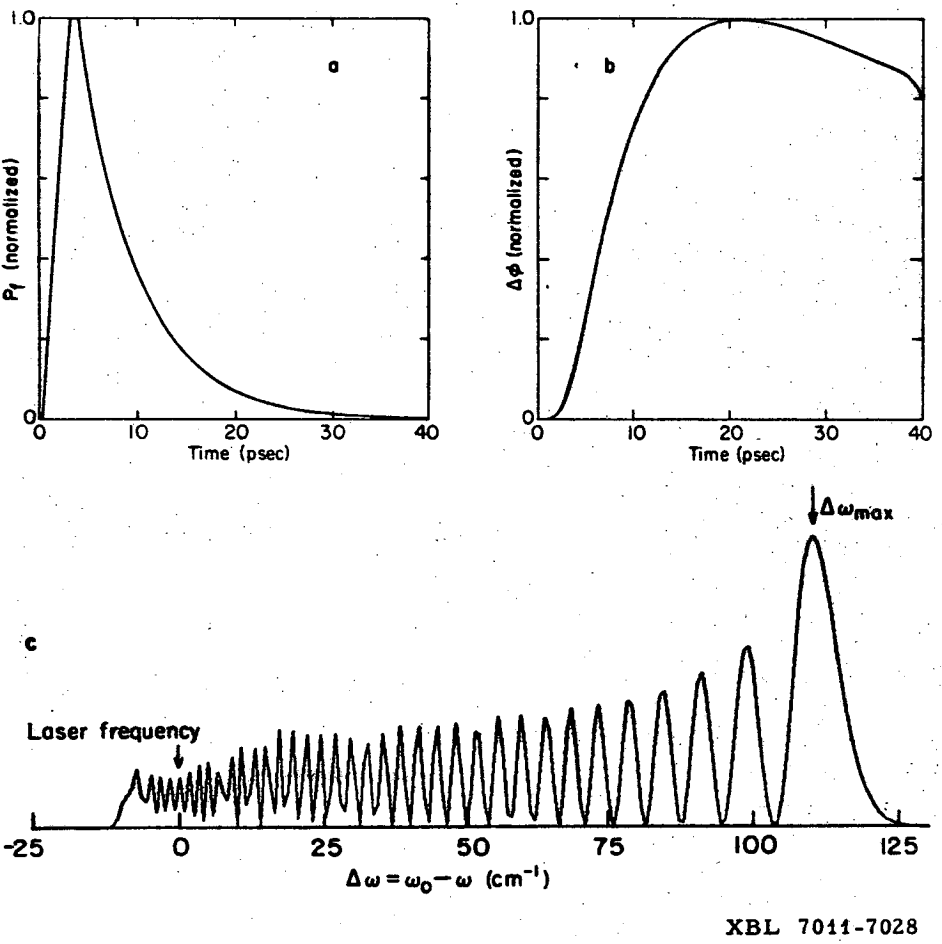
a
b
c
P_f (normalized)
$\Delta\phi$ (normalized)
Time (psec)
$\Delta\omega_{max}$
Laser frequency
$\Delta\omega = \omega_0 - \omega$ (cm^{-1})
XBL 7011-7028

Fig. 6

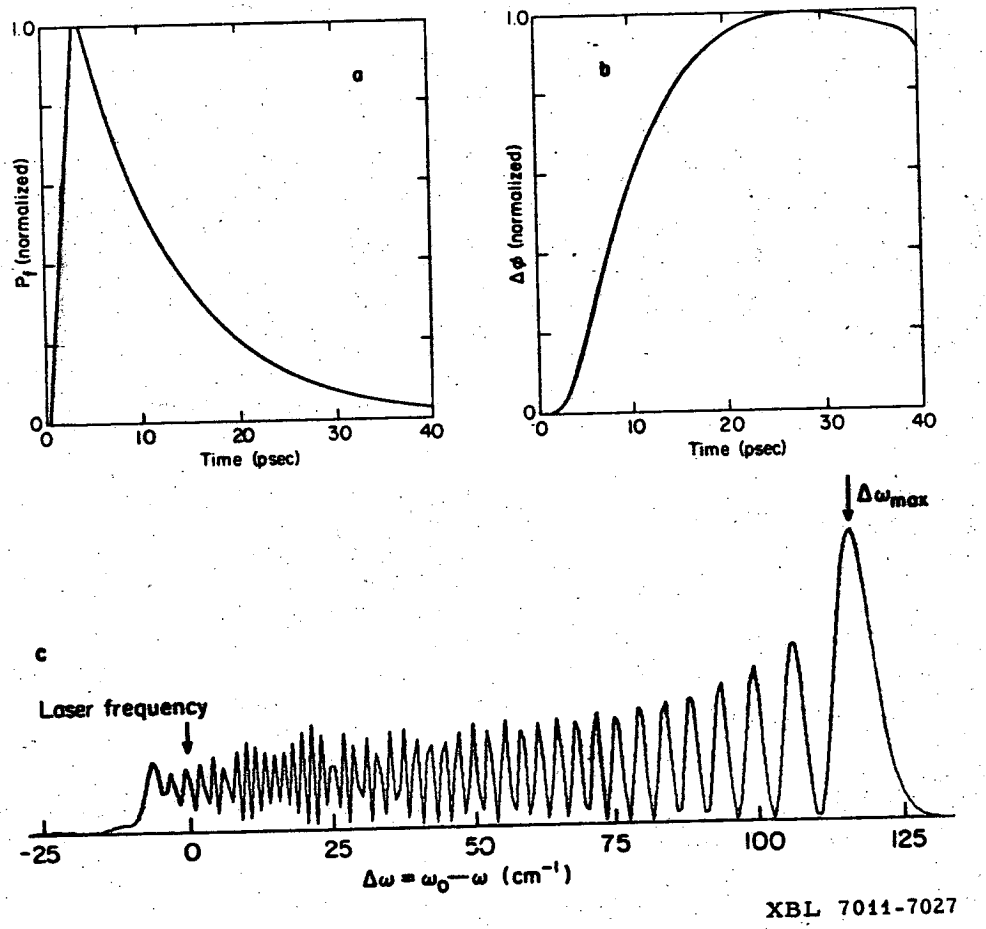
a
b
c
P_f (normalized)
$\Delta\phi$ (normalized)
Time (psec)
$\Delta\omega_{max}$
Laser frequency
$\Delta\omega = \omega_0 - \omega$ (cm^{-1})
XBL 7011-7027

Fig. 7

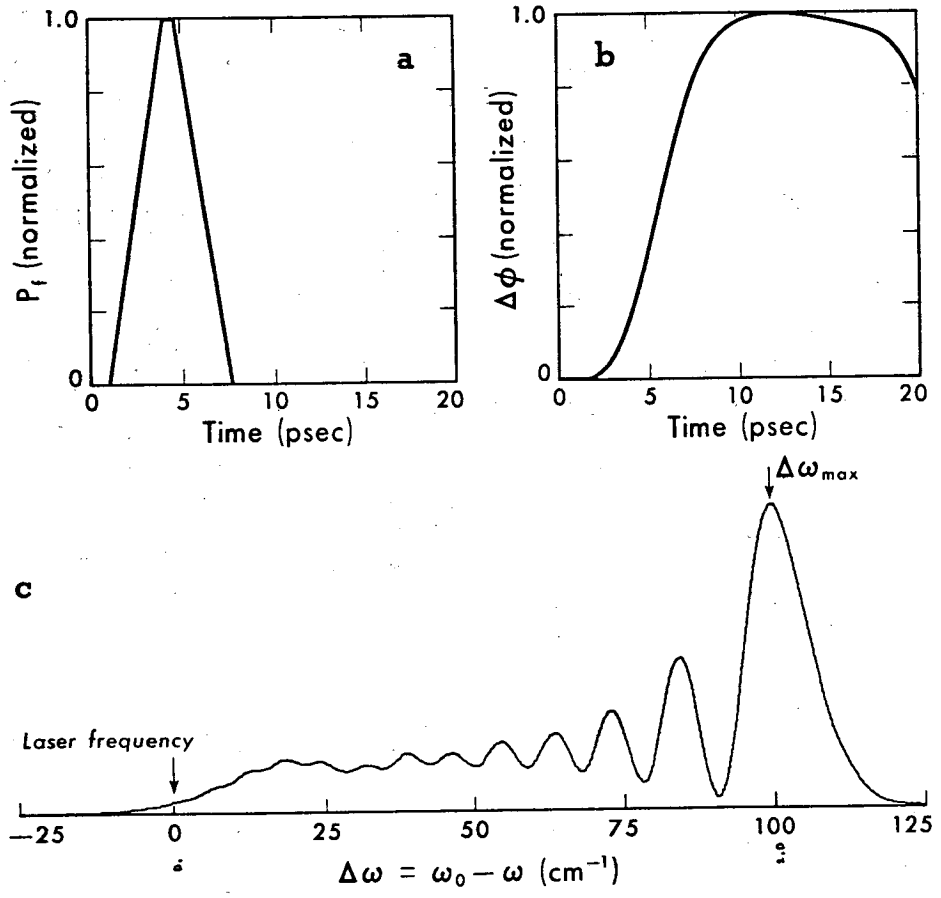

XBL 7011-7026

Fig. 8

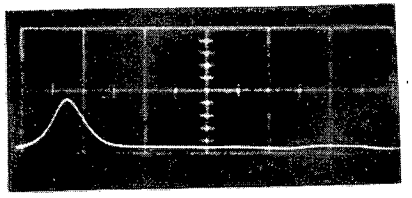

Time Scale:
10 nsec/div.

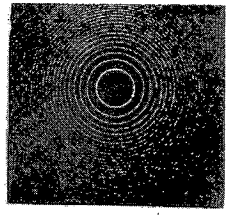

Free Spectral Range:
$\frac{1}{2L} = .4\ cm^{-1}$

XBB 715-2062

Fig. 9

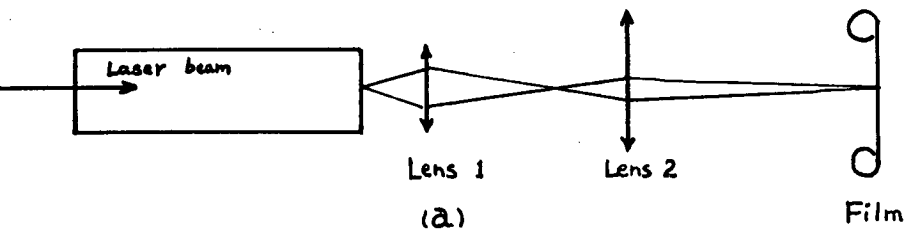

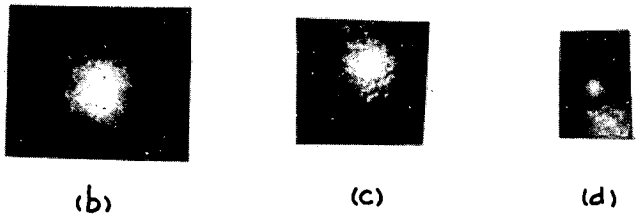

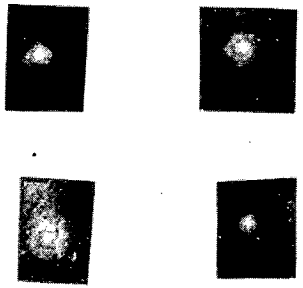

XBB 715-2063

Fig. 10

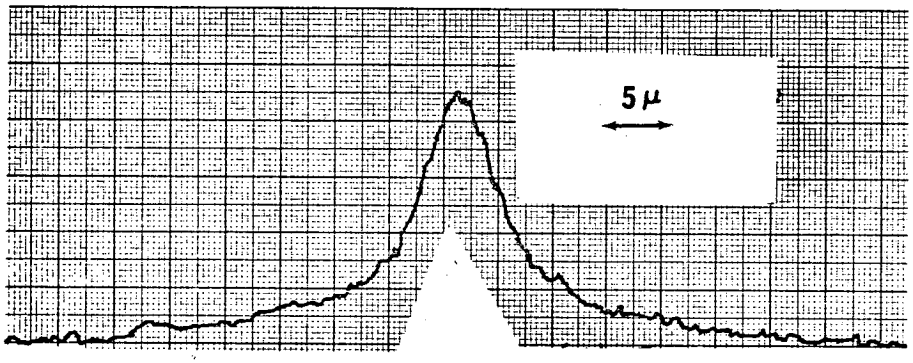

XBL715-6739

Fig. 11

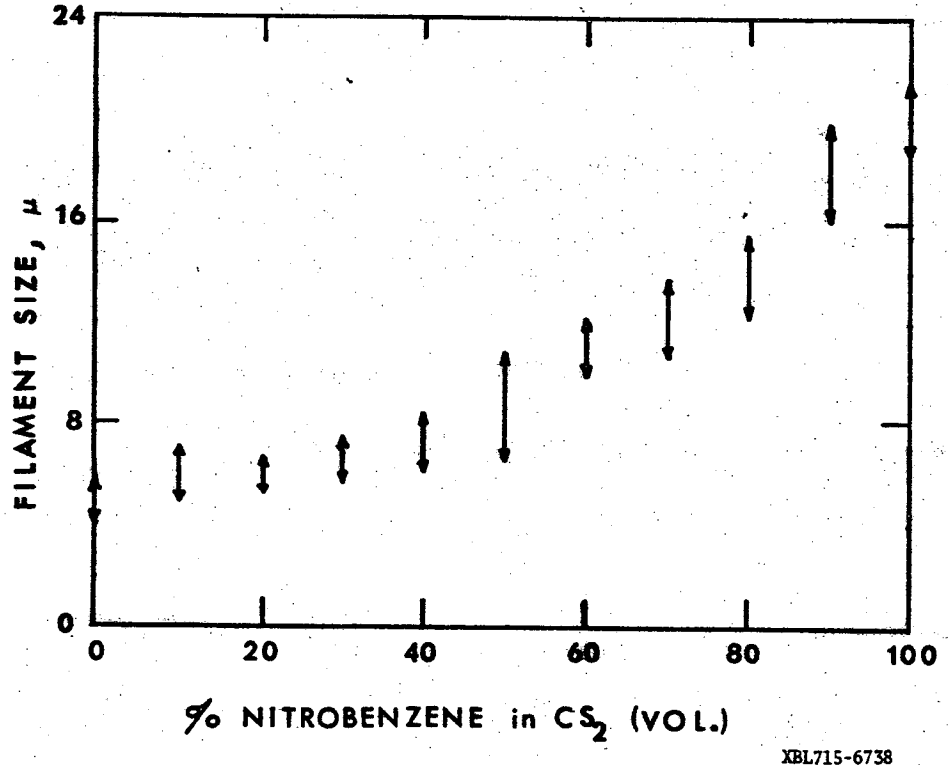
24
16
8
0
FILAMENT SIZE, μ
0
20
40
60
80
100
% NITROBENZENE in CS_2 (VOL.)
XBL715-6738

Fig. 12

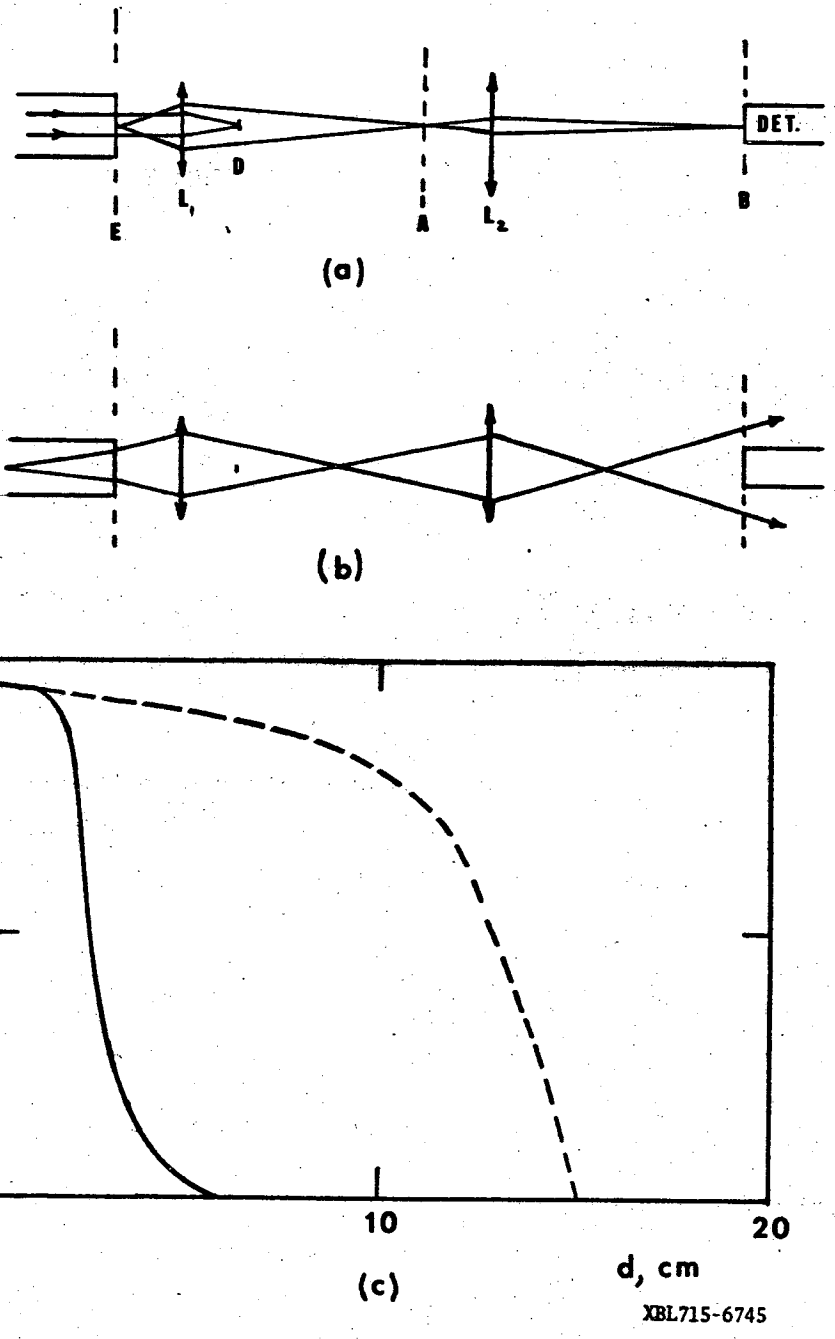
DET.
D
L_1
E
A
L_2
B
(a)
(b)
100
50
0
% DETECTED
0
10
20
d, cm
(c)
XBL715-6745

Fig. 13

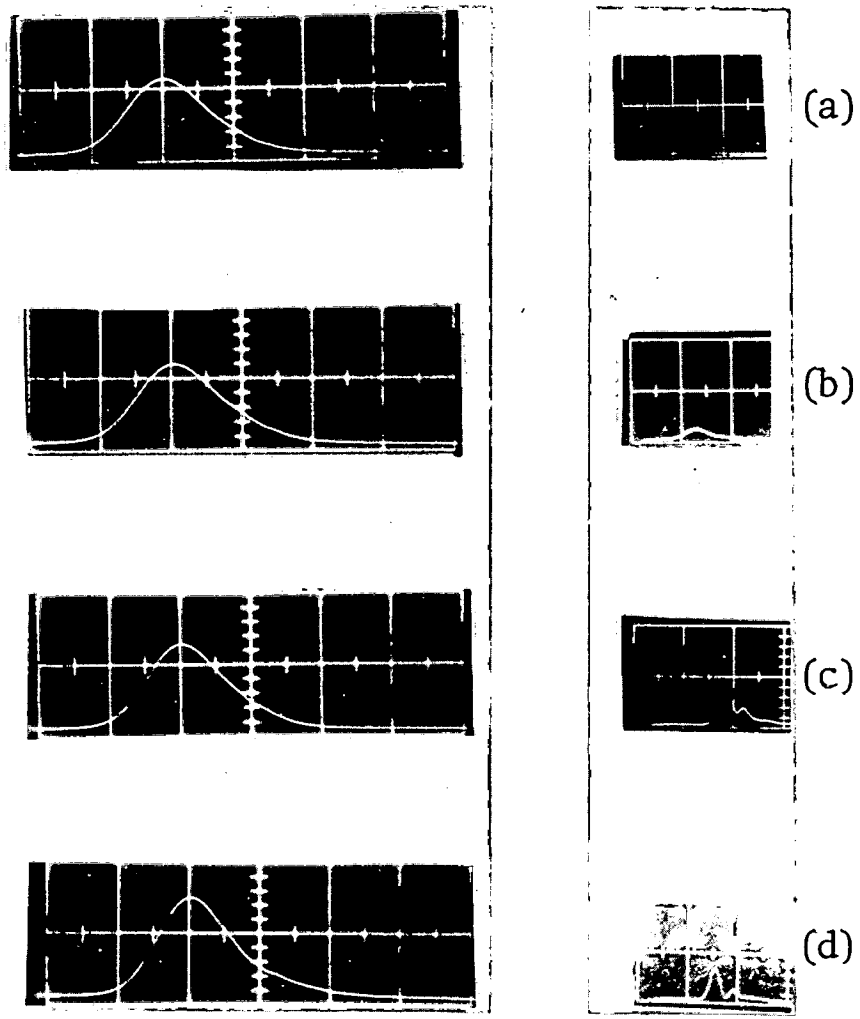

Input pulse
5 nsec/div

Filament pulse
2 nsec/div

XBB 715-2042

Fig. 14

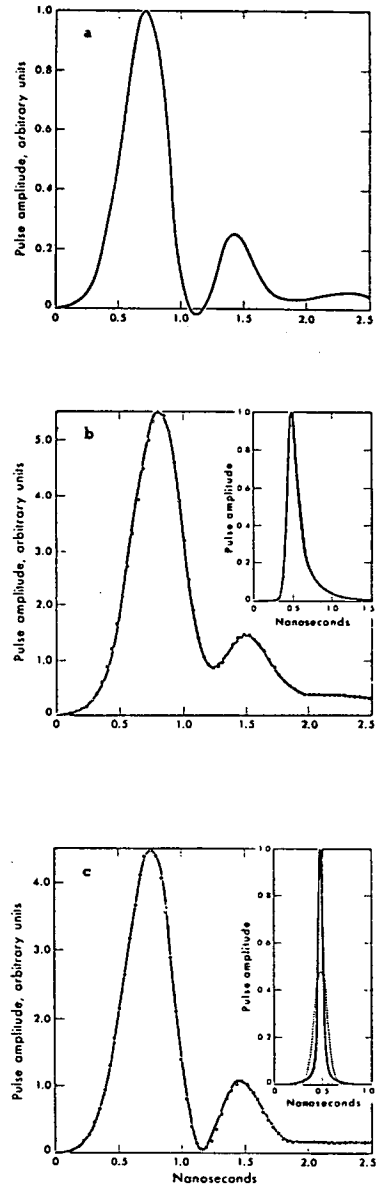

XBL715-6741

Fig. 15

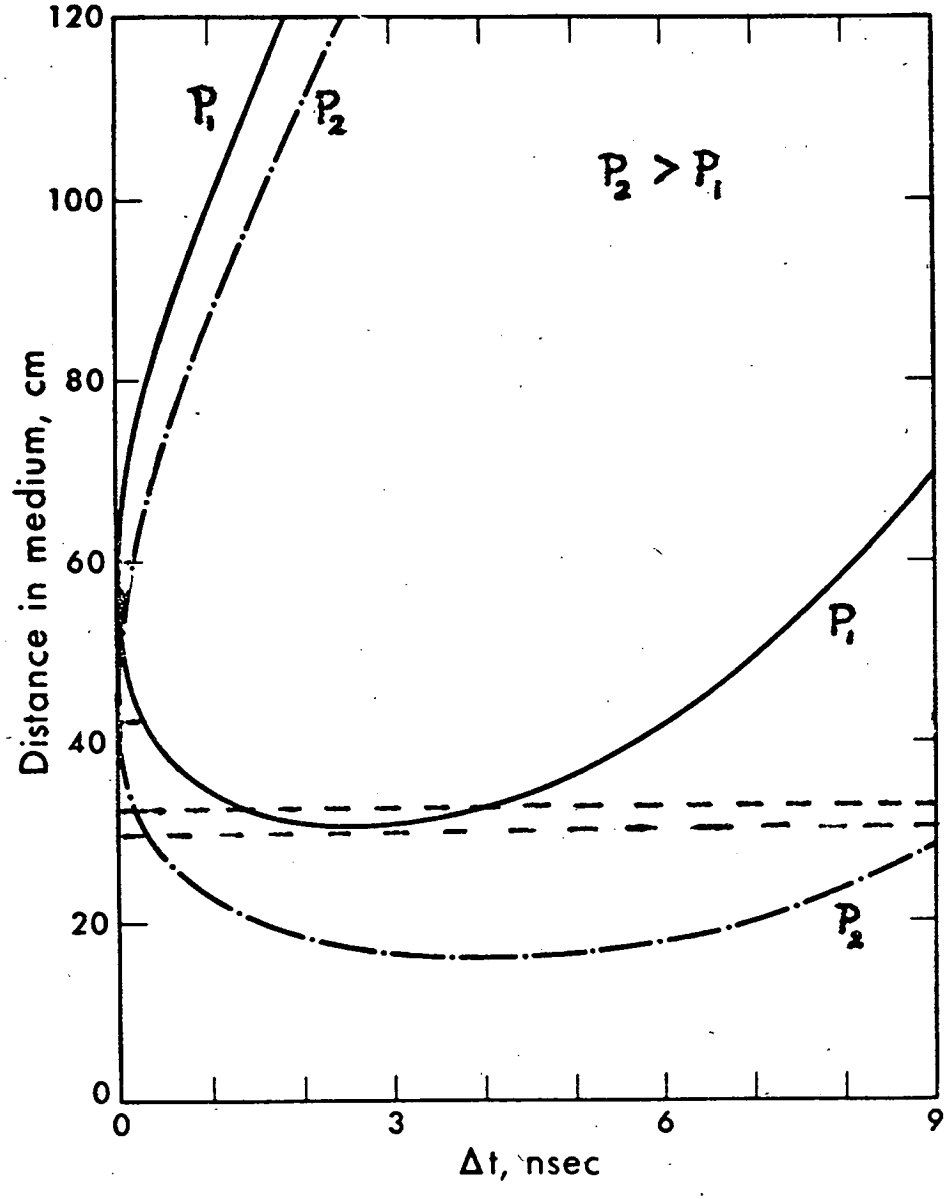

XBL715-6746

Fig. 16

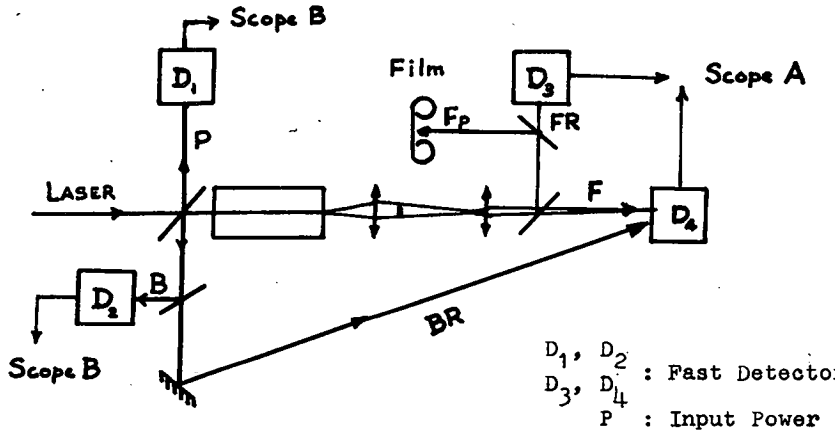

D_1, D_2 : Fast Detectors
D_3, D_4
P : Input Power
B : Backward Brillouin
BR : Backward Raman
FR : Forward Raman
F : Filament Pulse
F_p : Filament Picture

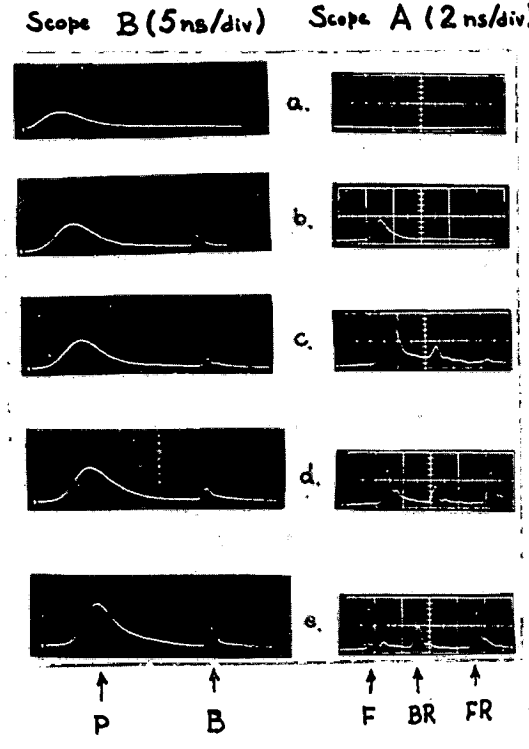

XBB 715-2064

Fig. 17

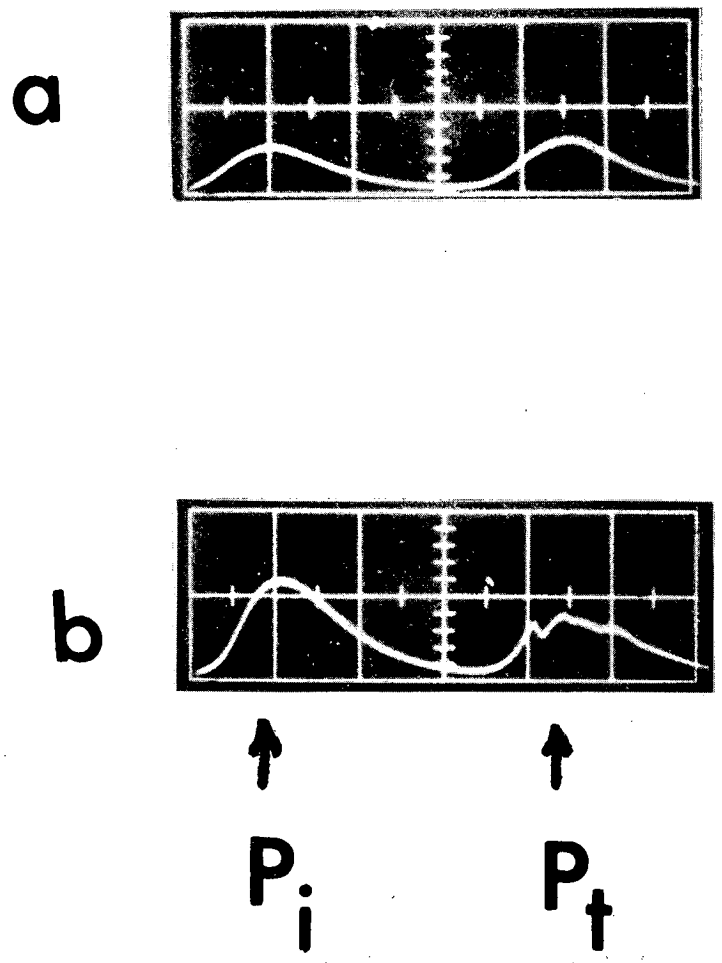

XBB 715-2065

Fig. 18

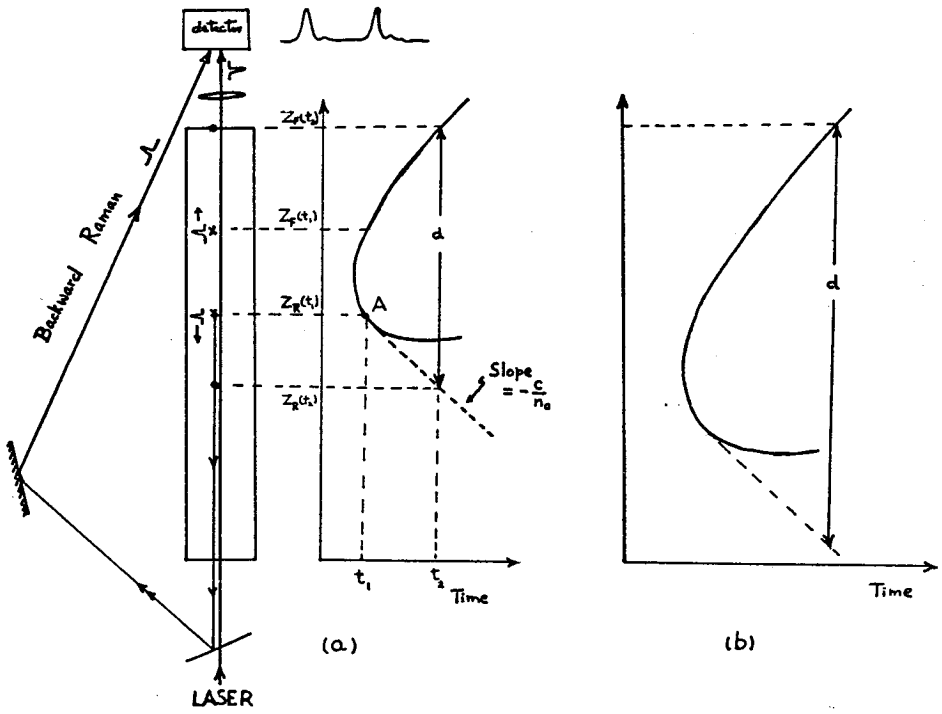

XBL715-6747

Fig. 19

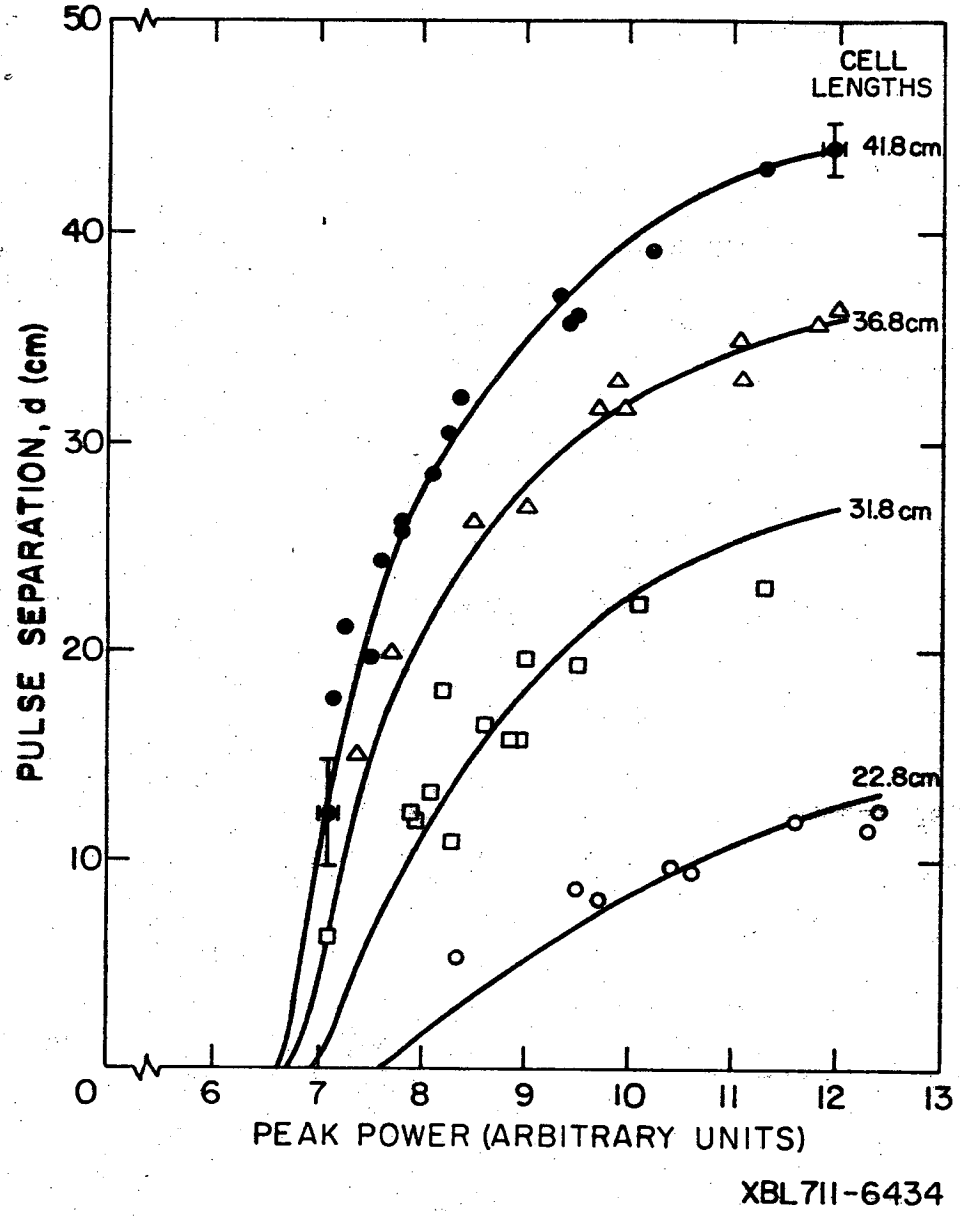
CELL LENGTHS
41.8cm
36.8cm
31.8cm
22.8cm
PULSE SEPARATION, d (cm)
PEAK POWER (ARBITRARY UNITS)
0
10
20
30
40
50
6
7
8
9
10
11
12
13
XBL711-6434

Fig. 20

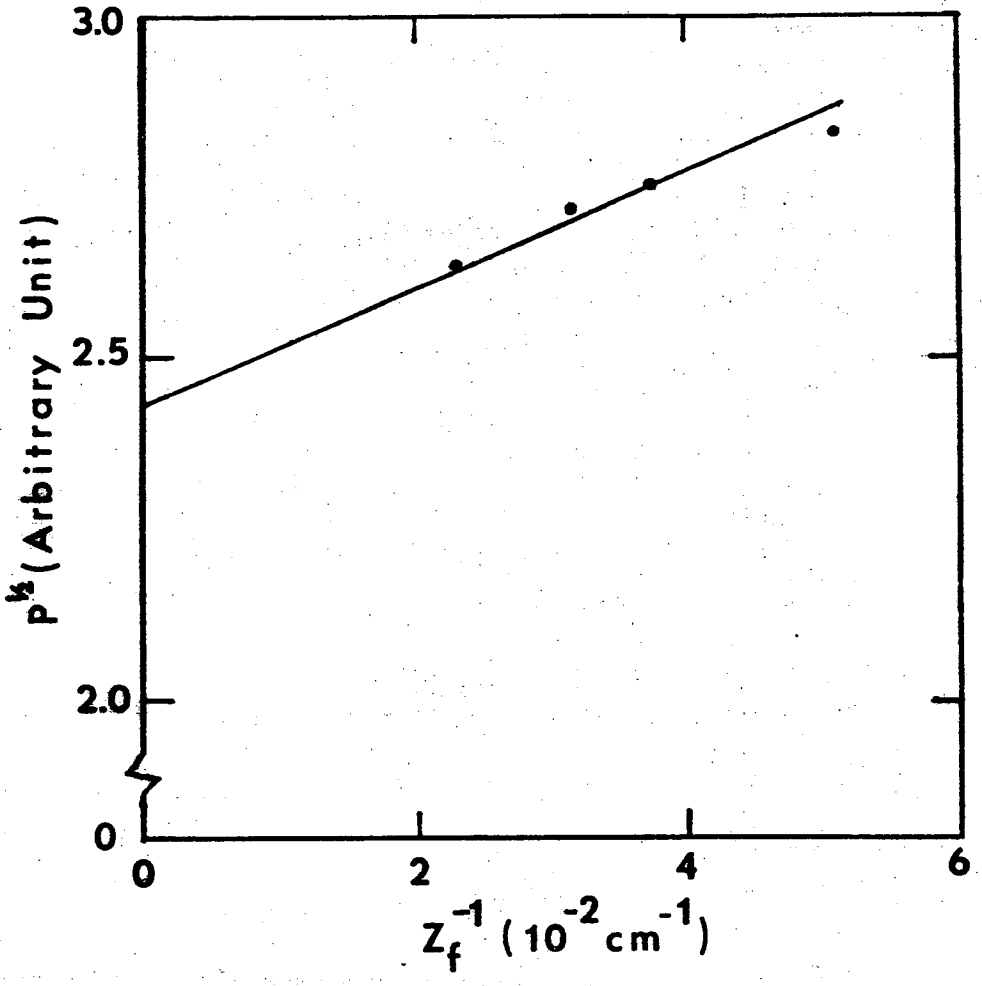
$p^{\frac{1}{2}}$ (Arbitrary Unit)
Z_f^{-1} (10^{-2} cm^{-1})
0
2.0
2.5
3.0
0
2
4
6
XBL715-6748

Fig. 21

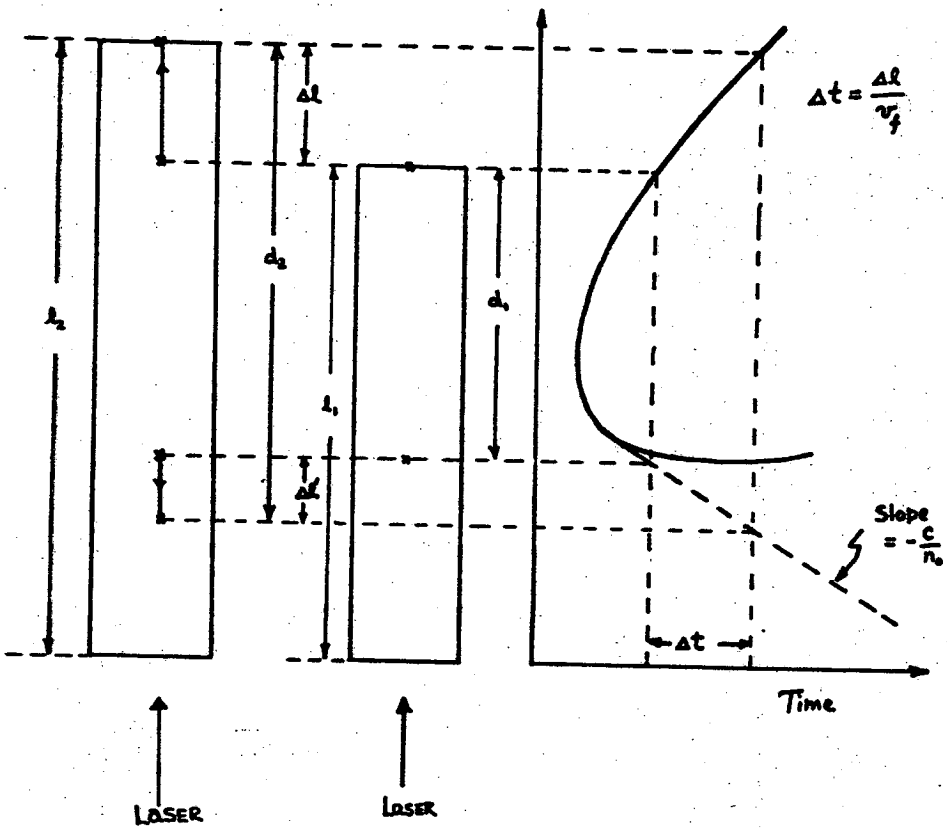

XBL715-6749

Fig. 22

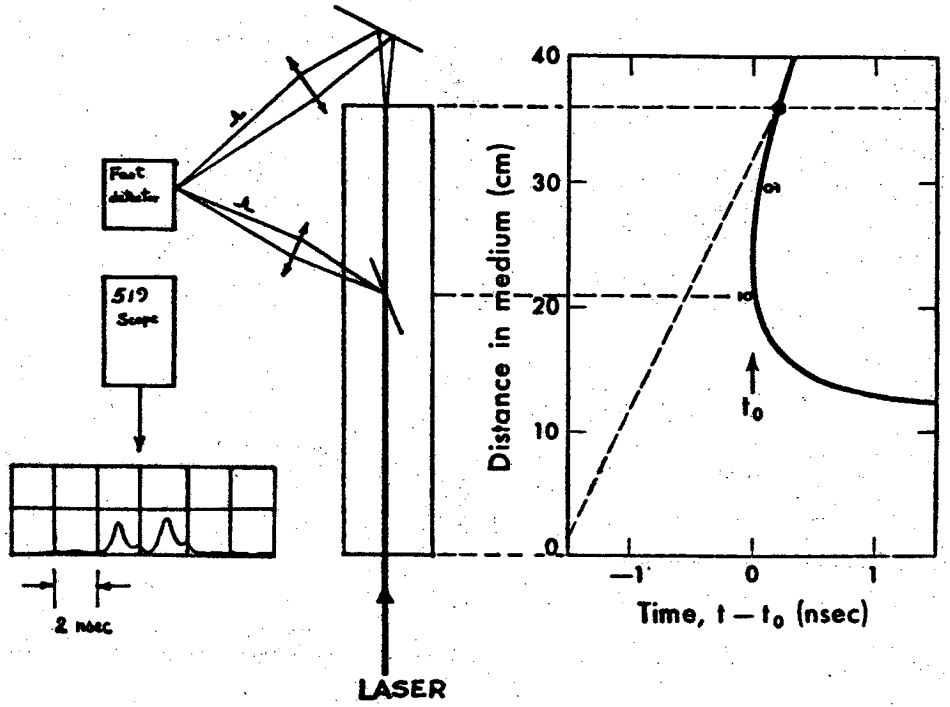

XBL715-6750

Fig. 23

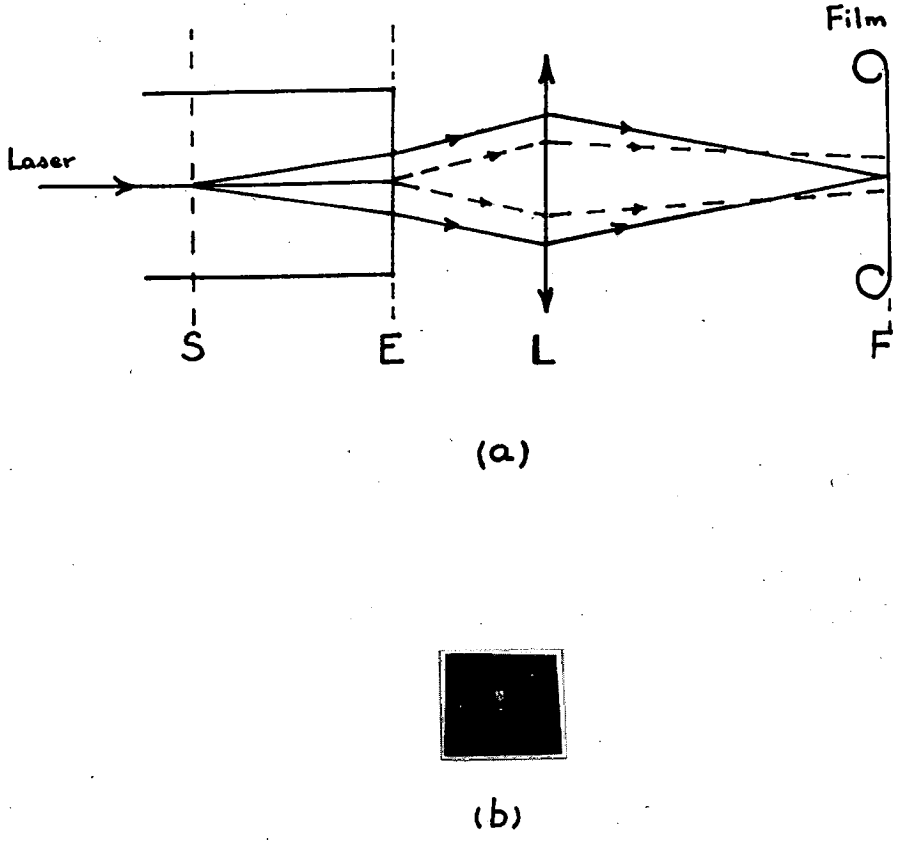

XBB 715-2066

Fig. 24

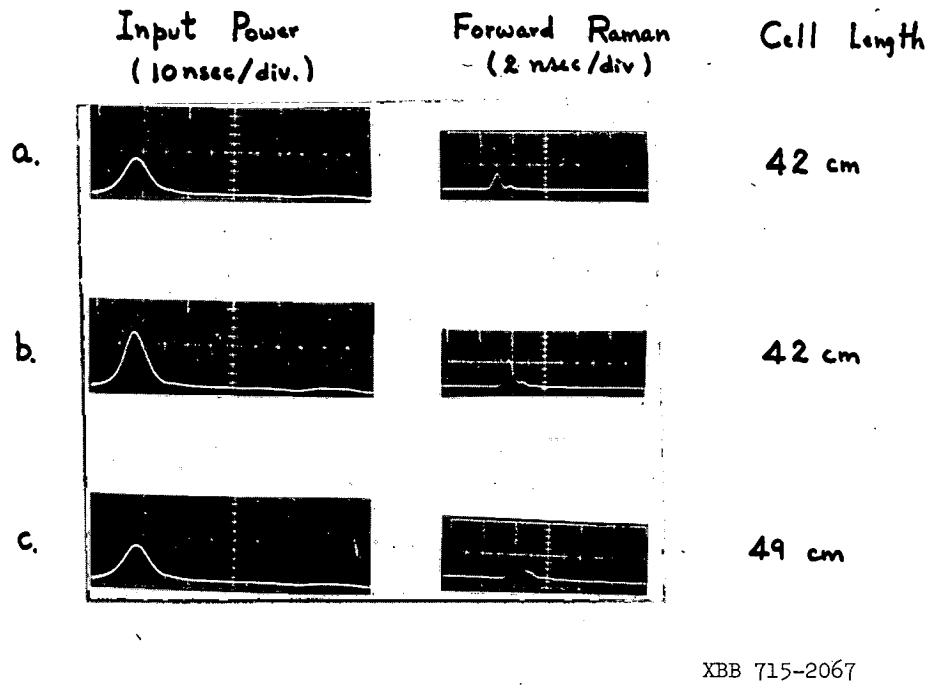

XBB 715-2067

Fig. 25

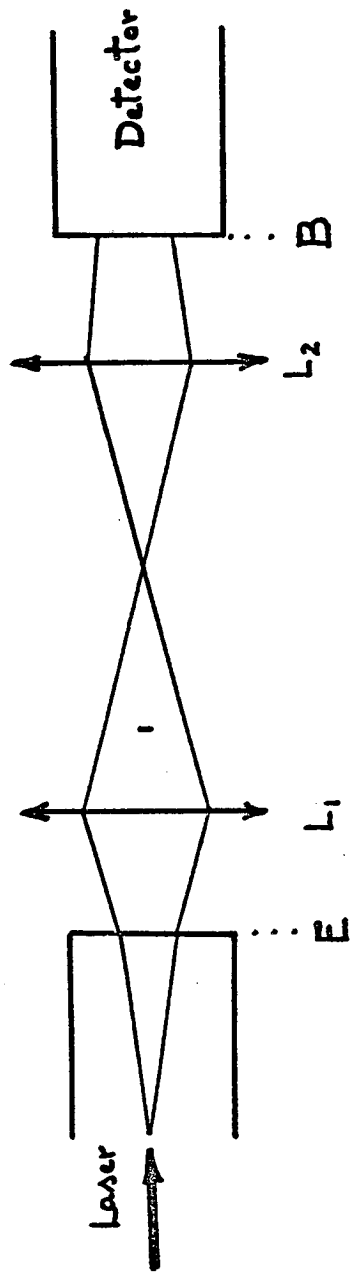

XBL715-6751

Fig. 26

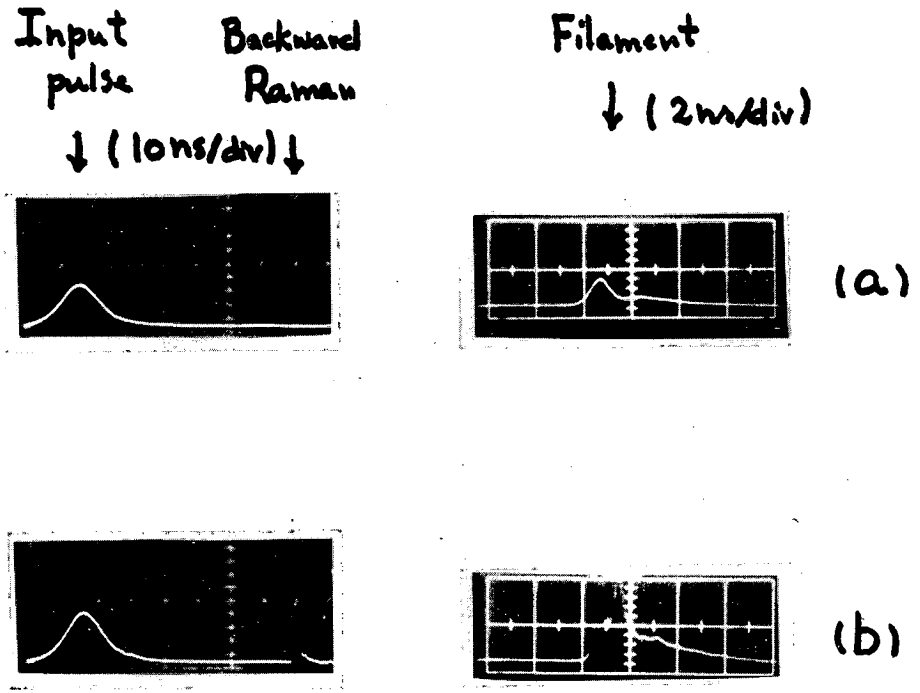

XBB 715-2068

Fig. 27

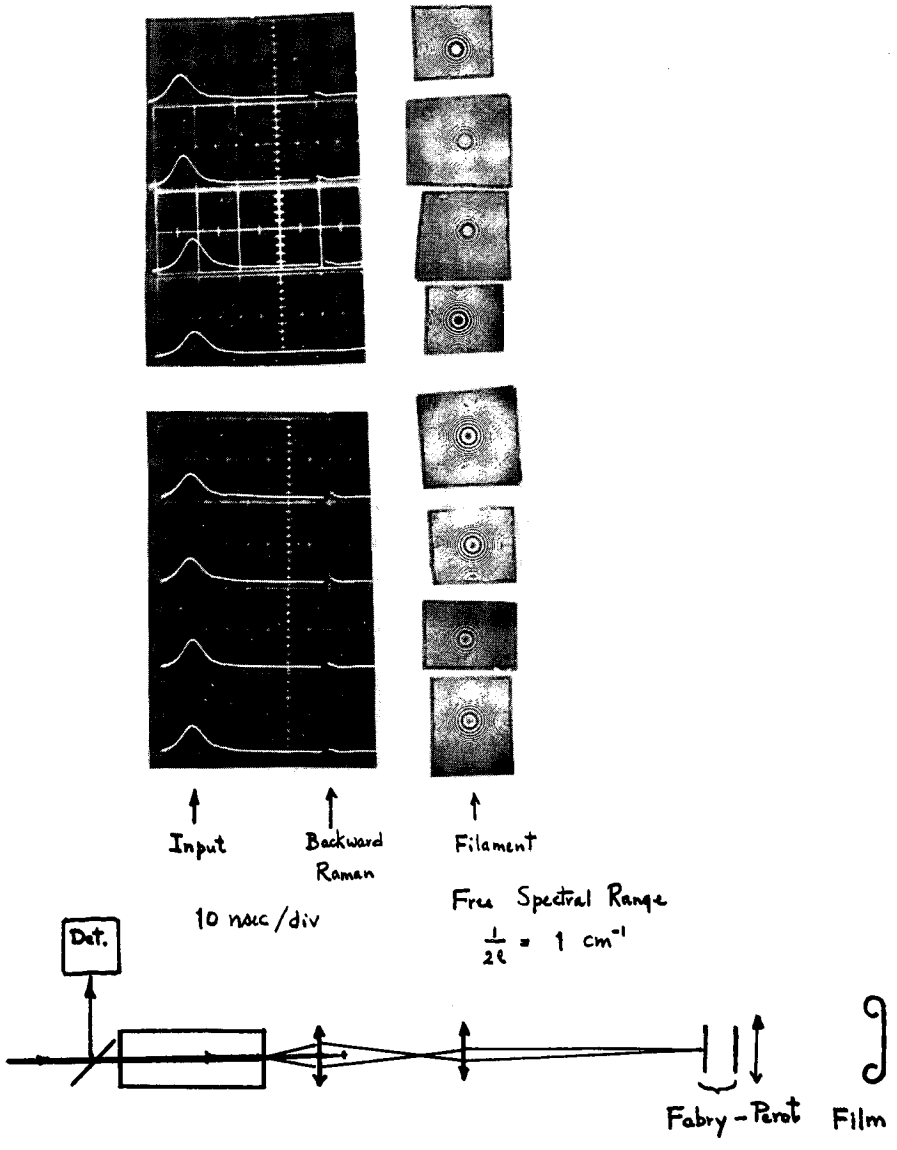

XBB 715-2069

Fig. 28

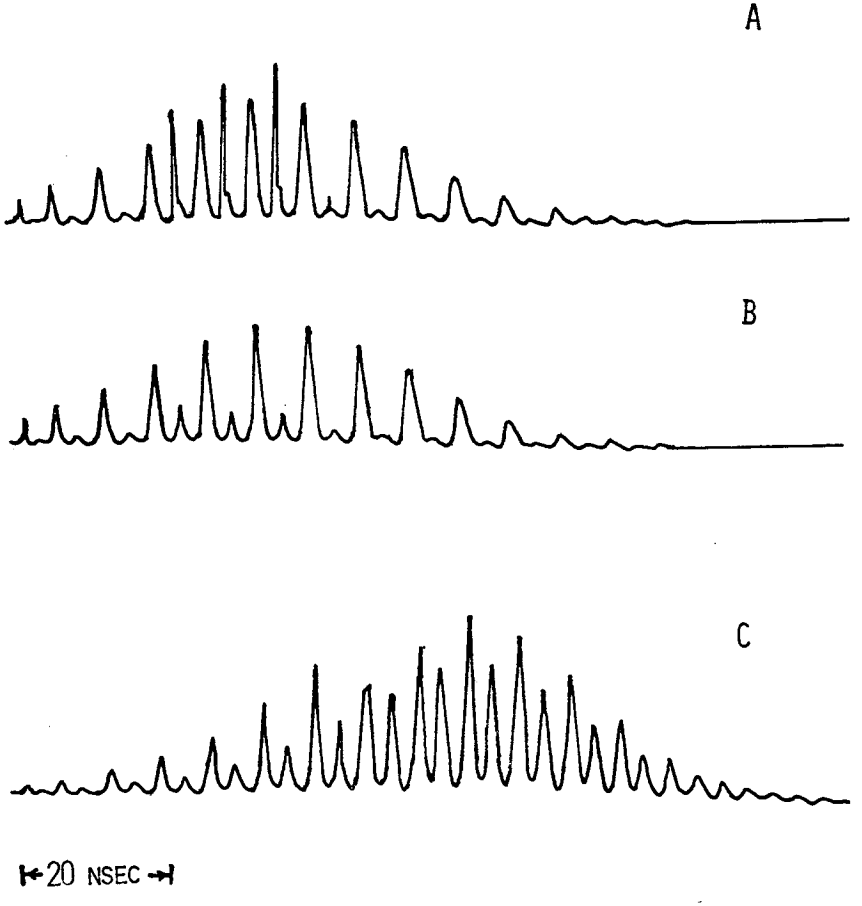

XBL 708-1726

Fig. 29

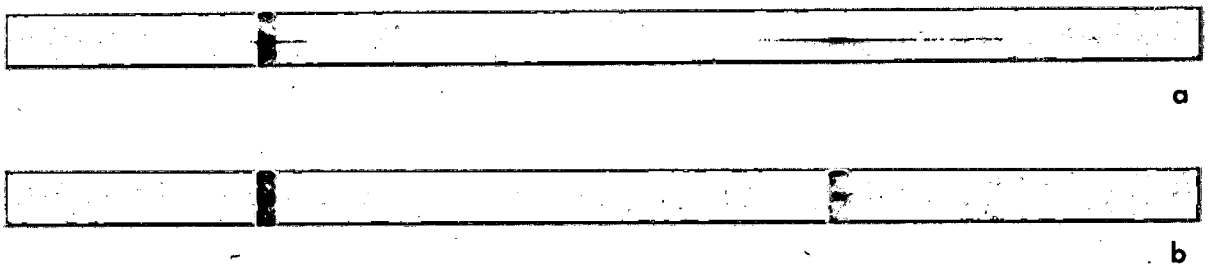

XBB 7010-4915

Fig. 30

TECHNICAL INFORMATION DIVISION
LAWRENCE RADIATION LABORATORY
UNIVERSITY OF CALIFORNIA
BERKELEY, CALIFORNIA 94720